AN ABSTRACT OF THE THESIS OF

John R. Herron for the degree of Doctor of Philosophy in Mechanical Engineering presented on December 14, 1989.
Title: Direct-Sampling Optical Techniques for the Study of Transient Combustion Events

Abstract approved: Redacted for privacy

Richard B. Peterson

Techniques have been developed for measuring the temperature, stable species concentrations, and atomic radical concentrations during a transient combustion event. They combine the features of direct sampling with two spectroscopic techniques to produce relatively simple diagnostic techniques to obtain time-resolved measurements. In this study, a transient event was provided by a propagating hydrogen/air flame. Stable species were detected downstream of the sampling orifice by electron impact fluorimetry, while temperatures and atomic hydrogen concentrations were measured by atomic resonance absorption spectroscopy. The calculation of stable species concentrations from time-varying fluorescence signals was straightforward, however conversion from absorption measurements to temperatures

and atomic radical concentrations required the development of a computer model of the radiation source and the absorption by the sample. The model of the source was validated by comparing predicted and recorded spectra of hydrogen Lyman-α emissions, while the absorption model for the sampled gas was tested by comparing the temperatures predicted by absorption measurements with those recorded at a range of known temperatures. These direct sampling spectroscopic techniques minimize time-history distortions inherent in other direct sampling techniques, and are capable of tracking local temperatures and species concentrations during the passage of a propagating flame front.

Direct-Sampling Optical Techniques for the Study of Transient Combustion Events

by

John R. Herron

A THESIS

Submitted to

Oregon State University

In partial fulfillment of the

requirements for the degree of

Doctor of Philosophy

Completed December 14, 1989

Commencement June, 1990

Thesis of John R. Herron

Approved:

Redacted for privacy

Associate Professor of Mechanical Engineering

In Charge of Major

Redacted for privacy

Head of Department of Mechanical Engineering

Redacted for privacy

Dean of Graduate School

Date thesis is presented December 14, 1989

Acknowledgement

I would like to thank Dr. Richard Peterson for initiating this project, and for his insights and guidance during its completion. I would also like to acknowledge financial support from the National Science Foundation, Grant No. CBT-8713328. Additional funding was provided from the Air Force Office of Scientific Research.

TABLE OF CONTENTS

LIST OF FIGURES

LIST OF TABLES

List of Symbols

Symbol	Definition
c	Speed of light
e	Charge on an electron
f	Oscillator strength
I_b	Current from electron gun
$I(\nu)$	Intensity as a function of frequency
k	Boltzman's constant
K_{0L}	Lamp centerline absorption coefficient
K_{0S}	Sample centerline absorption coefficient
$K(\nu)$	Frequency dependent absorption coefficient
L	Length of molecular beam
m	Molecular weight of atom
$\overline{M}$	Average molecular weight of the sampled gas
N	Number density
$\overline{R}$	Mixture gas constant
Q_{jk}	Molecular electron impact cross-section for the j to k transition
t	Time at which molecules arrive at the detector
T_0	Temperature of the sampled gas

T_L	Temperature of emitting-absorbing region in lamp
$\overline{U}$	Velocity of molecules in molecular beam
$\bar{\gamma}$	Average specific heat ratio of the sampled gas
Φ_{jk}	Radiation intensity due to j to k level electronic transitions
ν	Frequency
ν_0	Frequency at center of resonance line
$\Delta\nu_D$	Half width of Doppler broadening
θ	Solid angle
τ	Time at which molecule entered region of free molecular flow

DIRECT-SAMPLING OPTICAL TECHNIQUES FOR THE STUDY OF TRANSIENT COMBUSTION EVENTS

Chapter 1: INTRODUCTION

1.1 Overview

Any study of fundamental combustion processes is challenging due to the complex nature of flame chemistry. For instance, when a hydrocarbon is burned with air, there may be hundreds of separate reactions involved in the combustion. These reactions occur extremely rapidly due to both the elevated temperatures found in the flame, and the presence of highly reactive, short-lived intermediate species. Another factor which further complicates studies of flame chemistry is the sequence of combustion reactions is not fixed. Many reaction pathways exist and the relative importance of various reactions depend on initial fuel-mixture ratios, temperatures, and pressures. Therefore, to understand the chemistry of various flames, an instrument capable of measuring both stable and unstable species in specific flame environments is needed.

Previous investigations have provided extensive information about flame chemistry by employing a variety

of diagnostic techniques to study steady-state combustion. None of these techniques, however, is well suited to analyzing transient events such as flame ignition, extinction, or propagation. The difficulty in studying these processes lies in tracking their exceedingly rapid changes in local temperatures and species concentrations. For instance, in propagating flames, as the flame front passes a location, the entire course of combustion often occurs in less than a millisecond.

An ability to quantify the chemistry of transient flames could lead to a variety of technical advances including; increased efficiency and reduced pollutant formation in internal combustion engines and higher performance in jet engines.

This study demonstrates the ability to obtain concentrations of both stable and unstable species, along with temperatures, during transient events. This capability is achieved by combining an intrusive flame sampling technique, often referred to as direct sampling, with two well-studied spectroscopic methods of chemical analysis. In direct sampling, local mixture compositions are analyzed by continuously extracting gas from a flame through a small orifice and passing it into a vacuum chamber. The resulting rapid expansion freezes

chemical reactions, thus allowing the chemical composition of the flame to be determined by an analysis of the sampled gas.

In previous studies employing direct sampling, chemical species measurement has been performed by ion separation methods, which require the detector to be placed anywhere from 10 cm to 100 cm from the orifice. This placement produces a problem, however, when transient combustion events are studied. Because the time taken by molecules to traverse the distance to the detector decreases with increasing sample temperature, unacceptable time distortions may occur when events with extremely rapid temperature increases are studied. Such distortions were minimized in this investigation by using spectroscopic techniques to analyze the gas within a few millimeters of the orifice.

The first of the spectroscopic techniques was employed to measure the concentrations of stable species during the propagation of a flame through a hydrogen/air mixture. In this technique, fluorescence from the sampled gas was induced by directing a well-collimated electron beam through the free jet from the sampling orifice. Time-resolved concentrations of N_2, O_2, and H_2O were then obtained by recording the fluorescence intensity at appropriate frequencies.

The second spectroscopic technique allowed for the measurement of both atomic free radical concentrations and temperatures in transient flames. Measurement of atomic radicals is of interest because of their major role in determining combustion rates and flame propagation speeds. In the current investigation, the time-resolved concentrations of hydrogen free-radicals produced in a propagating hydrogen/air flame were measured by means of atomic resonant absorption spectroscopy. In this technique, the amount of radiation absorbed at hydrogen's Lyman-α resonant frequency was recorded in a light beam passing through the sample jet. Calculation of concentrations from these measurements, however, was complicated by frequency-dependent variations within the resonant lines. Therefore, a computer model of the absorption was developed to perform the necessary computations.

Resonant absorption measurements were also used to obtain sample temperatures. This was accomplished by adding a small fraction of a monatomic inert gas (krypton) to the gas mixture, and recording its time-varying resonant absorption during combustion.

1.2 Organization

Due to the differences in the spectroscopic analysis

techniques, the main body of this thesis is presented in three chapters. Chapter two discusses the features of the direct sampling technique, while chapter three describes experiments employing direct sampling electron impact fluorimetry to measure stable species. This chapter contains sections discussing electron impact phenomena, the experimental apparatus, and the results.

Chapter four is devoted to the measurement of temperatures and free radicals by direct sampling atomic resonance absorption spectroscopy. The computation of mole fractions using this technique is much more complicated than that for electron impact experiments, therefore a major portion of this chapter discusses the development of a computer code to perform these calculations. Other sections in this chapter cover; atomic resonance absorption spectroscopy, the experimental apparatus, the validation of the computer model, transient temperature measurements, and the measurement of hydrogen free radicals.

Conclusions and recommendations for further work are presented in chapter five.

Chapter 2: DIRECT SAMPLING

The technique of direct sampling has yielded much new and valuable information concerning combustion. When coupled with molecular beam formation and mass spectrometry, detailed knowledge of temperatures and chemical species is provided as seen in the works of Deckers and Van Tiggelen (1959); Milne and Green (1966); Peeters and Mahnen (1972); Knuth (1973); Biordi 1977); and Lazzara, Biordi, and Papp (1973). Although this technique is a powerful tool in the study of steady state flame systems, it has only been rarely used in the study of transient phenomena (Peterson et al., 1984; Lucas et al., 1984a; Lucas et al., 1984b) due to an inherent shortcoming known as molecular beam overrun.

To describe beam overrun, the formation and characteristics of the molecular beam must be addressed. In direct sampling, the gas passing through the orifice produces a supersonic free jet into the vacuum chamber. A diagram of a free jet is presented in Fig. 1. Such jets have a unique structure characterized by a central hypersonic-flow region of low temperature and density which is surrounded by an oblique shock wave. A normal shock also exists, however if the pressure in the vacuum chamber is low, the position of this shock is far

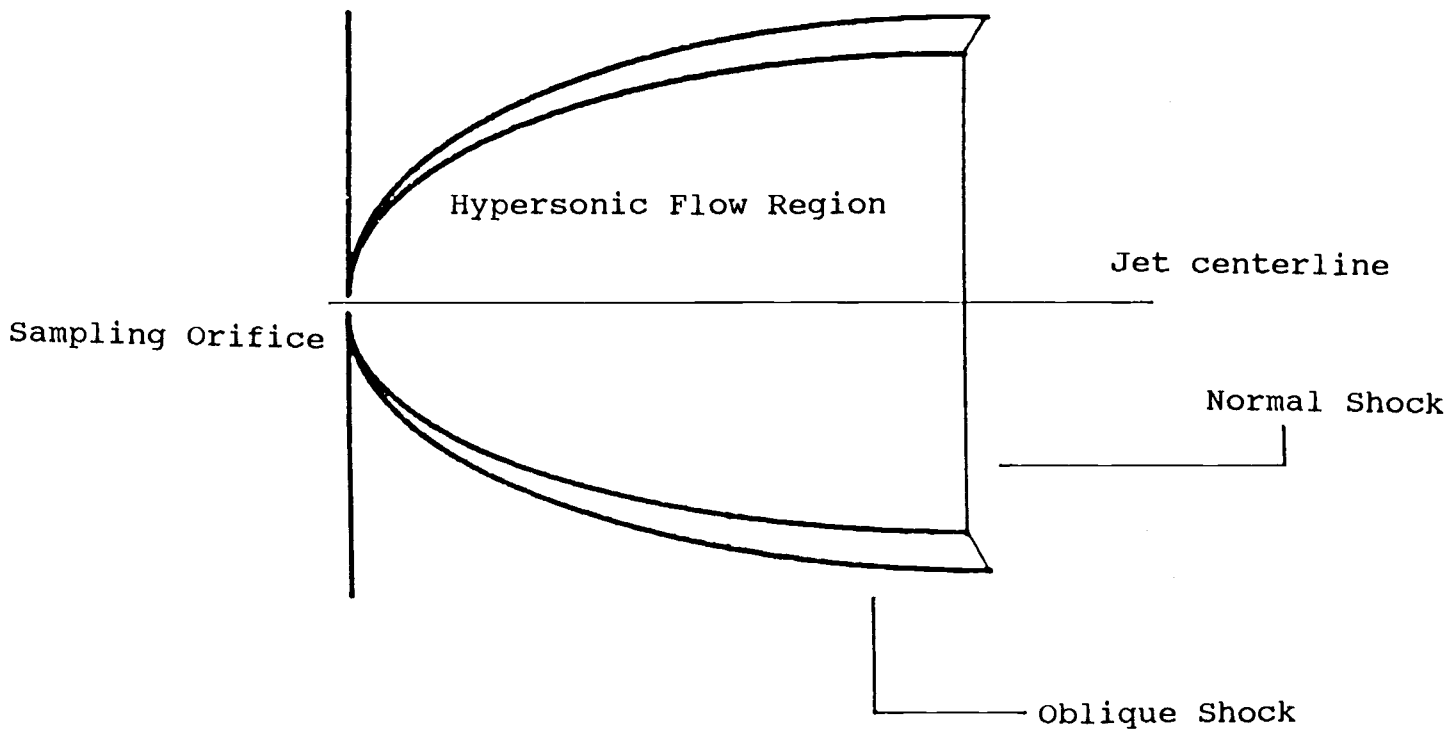

Fig. 1 Structure of a free jet.

downstream from the orifice. In mass spectrometry, the edges of the free jet are skimmed off, leaving the center portion to form a beam in which the molecules are all moving in the same direction at a nearly uniform velocity. The formation of free jets and molecular beams has been extensively studied (Kantrowitz and Grey, 1951; Ashkenas and Sherman, 1966; Hammel and Willis, 1966; Bier and Hagena, 1963; Fenn and Deckers, 1963; Scott and Drewry, 1963). The mean velocity of molecules in the molecular beam may be given by (Smith, 1982)

$$\overline{U} = \left(\frac{2\overline{\gamma}}{\overline{\gamma}-1} \; \frac{\overline{R}}{\overline{M}} \; T_0 \right)^{\frac{1}{2}} \qquad (1)$$

where $\overline{\gamma}$ is the average specific heat ratio of the sampled gas, $\overline{R}$ is the gas constant, $\overline{M}$ is the mean molecular weight of the sample, and T_0 is the source temperature.

Molecular beam overrun refers to a situation in which, due to changes in the source conditions, some molecules in the beam are able to arrive at the detector before other molecules which were sampled earlier. This situation can occur in cases, such as transient combustion, in which an extremely rapid temperature increase takes place. The preceding equation demonstrates a rise in T_0 creates a corresponding increase in $\overline{U}$, thus indicating molecules sampled from a

hot gas will traverse the distance to the detector in less time than those removed from a cooler gas. If a sufficiently rapid increase in source temperature occurs, molecules from the hot gas can overtake those sampled from the cooler gas, thus destroying the time ordering of the analysis.

To characterize the rate of temperature increase for which a particular instrument experiences beam overrun, the following treatment has been presented (Smith, 1982). During the measurement of a transient event, the time at which molecules arrive at the detector is given by

$$t = \tau + \frac{L}{\bar{U}} \tag{2}$$

where τ is the time a molecule enters the region of free molecular flow (the point in the free jet at which the flow can no longer be considered a continuum), and L is the length of the region. Overrun occurs when, for some interval during sampling, increasing τ leads to decreasing t. This means the condition of no overrun may be explicitly stated as $dt/d\tau \geq 0$. Assuming T_0 to be a time dependent quantity, the limiting case of $dt/d\tau = 0$ may then be written,

$$\frac{dT_0}{d\tau} = \frac{T_0^{3/2}}{L} \left(\frac{8\bar{\gamma}}{\bar{\gamma} - 1} \frac{\bar{R}}{\bar{M}} \right)^{\frac{1}{2}} \tag{3}$$

It may be shown that the rate of temperature increase which will cause beam overrun in a mass spectrometer is on the order of 10^6 K/s. This means the response rate of these instruments is insufficient to prevent overrun when transient flames are studied since many processes produce rates of increase greater than 10^7 K/s. In this study, to increase the time resolution of direct sampling, the sample was analyzed within a few millimeters of the orifice.

Chapter 3: DETECTION OF STABLE SPECIES

3.1 Electron Impact Fluorimetry

It is possible to detect chemical species very near the orifice by employing spectroscopic techniques instead of the ion separation used in mass spectrometers. The first spectroscopic analysis was performed by electron impact fluorimetry (EIF). In this technique, fluorescence is induced by passing an electron beam through a low density gas. Electron impact on molecules in the gas create ions and free radicals, some of which have their electrons in high energy states. Fluorescent radiation is then emitted as these electrons fall back to lower energy levels. By recording the frequency and intensity of the emissions, local values of the composition, density, and temperature of the gas may often be determined. This technique provides for local analysis since, if the beam is well collimated, fluorescence is only induced in a narrow cylinder along the beam path. A discrete volume may then be studied by optically selecting a short portion of the fluorescing region for analysis.

EIF is a well-investigated technique which has been used throughout much of this century. A review of the early applications is presented by Massey and Burhop

(1969). In the 1950s, EIF was first used as a non-intrusive diagnostic tool for the study of gas flows (Schumacher and Gadamer, 1959; Muntz, 1962), then soon afterward it was employed to study the characteristics of free jets (Robben and Talbot, 1966; Marrone, 1967; Coe et al., 1980; Dekoven et al., 1981; Hernandez et al., 1982). It should be noted, however, that all of these investigations involved studies of steady state flows of a single constituent gas.

Findings from previous studies which are relevant to transient mole fraction measurements may be summarized as follows:

* The frequency spectrum from each emitting species is unique. In the visible and ultraviolet region (200 nm - 700 nm), spectra exhibit intensity peaks corresponding to the energies of the species' allowed electronic transitions. For atomic species, these peaks are very narrow, while for diatomic and polyatomic molecules, the peaks are broadened due to molecular vibration and rotation effects. In many cases, it is possible to identify the composition of a sample by recording its fluorescence spectrum.

* The residence time of electrons in excited states is very short. This means the fluorescence process introduces essentially no time distortions when EIF is used to study transient events.
* Fluorescent intensities for each peak in an emission spectrum change proportionally with changes in emitter density. This is a valid approximation because the density of the jet is so low that little attenuation of the beam, and little destruction of emitters by radiationless collisions (quenching) occur. The directional radiation intensity resulting from electron impact excitation of a molecule's j → k transition may therefore be given by; (Ocheltree, 1973; Massey and Burhop, 1969)

$$\Phi_{jk}(\theta) = \frac{I_b}{e} N \Delta x \frac{d}{d\Omega} (Q_{jk}(\theta)) \qquad (4)$$

where θ is a solid angle, I_b is the electron current in the volume, e is the electron charge, N is the gas number density, Δx is the length of the incremental volume, Ω is the emission angle, and Q_{jk} is the molecular electron impact cross-section for the j → k transition.

3.2 Experimental

The diagnostic portion of the direct sampling

electron impact fluorimetry (DSEIF) apparatus is shown in Fig. 2. The main chamber consisted of a hollow aluminum cube 15.24 cm on a side with each face providing access to the interior region. Front, top, and side access ports were used to house a gas sampling orifice, a low voltage electron gun (<200 V), and an optical viewing port, respectively. The back of the chamber exhausted to a 1200-l/s oil diffusion pump.

The electron gun was constructed following the design described by Erdman and Zipf (1982). A diagram of the gun is shown in Fig. 3. The body consisted of a filament holder, an extractor plate, and four focusing lenses, each constructed from stainless steel. Electrical connections allowed the plates to receive various electrical potentials, and, in addition, were isolated by means of sapphire spacers. A 0.1275-mm tungsten filament electron source was positioned so that a portion of the filament crossed the gun centerline, 0.1 mm from the grid plate orifice. Pressures in the electron gun chamber were maintained below 0.001 Pa (10^{-6} Torr). At a 130-V beam energy, maximum beam current was delivered with the settings listed in Table 1.

Several experimental configurations were employed in this study. The apparatus shown in Fig. 2 was used to

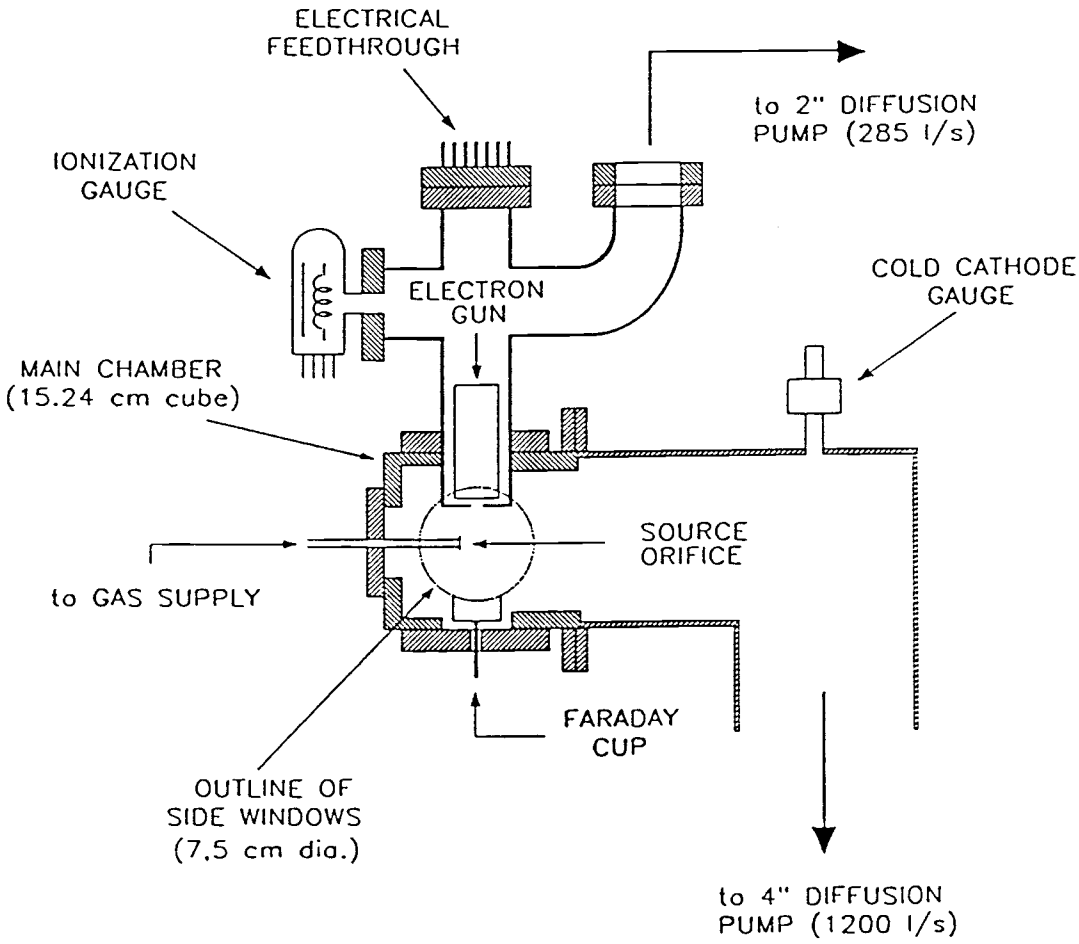

Fig. 2 Diagram of the DSEIF apparatus.

Dimensions of Electron Gun

O.D. of Each Element = 3.5 cm
I.D. of Each Element = 1.5 cm
Extractor Plate Aperature = 2 mm
Lens 1 Aperature = 4 mm

Element	Thickness
Filament Holder	12.0 mm
Extractor Plate	6.0 mm
Lens 4	6.0 mm
Lens 3	13.5 mm
Lens 2	6.0 mm
Lens 1	11.2 mm

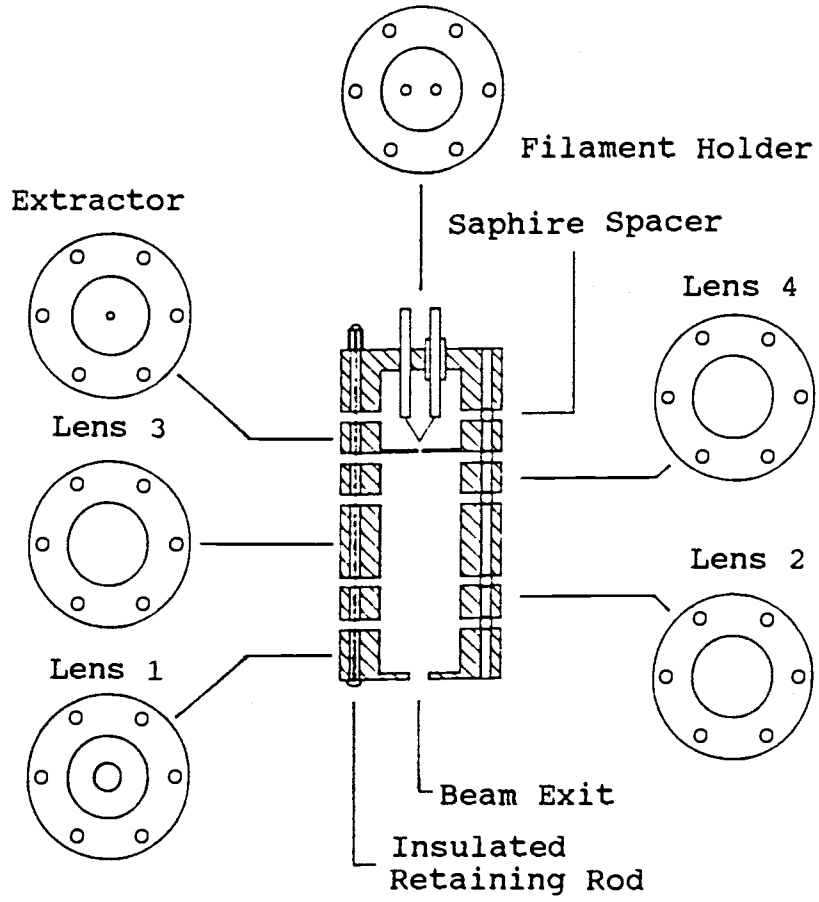

Fig. 3 Diagram of an electron gun.

Table 1

Settings for Maximum Electron Beam Current at -130 eV

Filiment-holder/filiment voltage	-130 V
Grid plate voltage	-125 V
Lens 1 voltage	730 V
Lens 2 voltage	0 V
Lens 3 voltage	800 V
Ground plate voltage	0 V
Beam width through free jet	2 mm
Filiment current	2 amps
Beam current	3×10^{-5} amps

obtain standard DSEIF reference spectra of N_2 (from air), O_2, H_2, and NO. In this configuration, a 4-mm O.D. glass tube was inserted through the front access port. To provide a sampling orifice, a brass foil possessing a 0.06-mm hole was affixed to the end of the tube. Gas at atmospheric pressure was supplied to the upstream side of the orifice, while a pressure of 0.07 Pa (5×10^{-4} Torr) was maintained in the vacuum chamber. The tube was positioned so that the orifice was 1.0 cm from the centerline of the electron beam.

Figure 4 details the various source arrangements employed in this investigation. Elevated temperature reference spectra were obtained using sources 4a and 4b, while source 4c was used in transient combustion experiments. A reference spectrum from water was obtained by attaching the source arrangement shown in Fig. 4a to the front access port. Sampling was performed using a quartz plate with an indented cone orifice. The orifice diameter was 0.120 mm. Copper coils were attached to the inside of the insert for cooling during high temperature runs. Superheated water vapor was supplied to the inner tube, with the tube exit being located approximately 0.5 cm from the orifice plate. Temperatures of the vapor were measured with a chromel-alumel thermocouple.

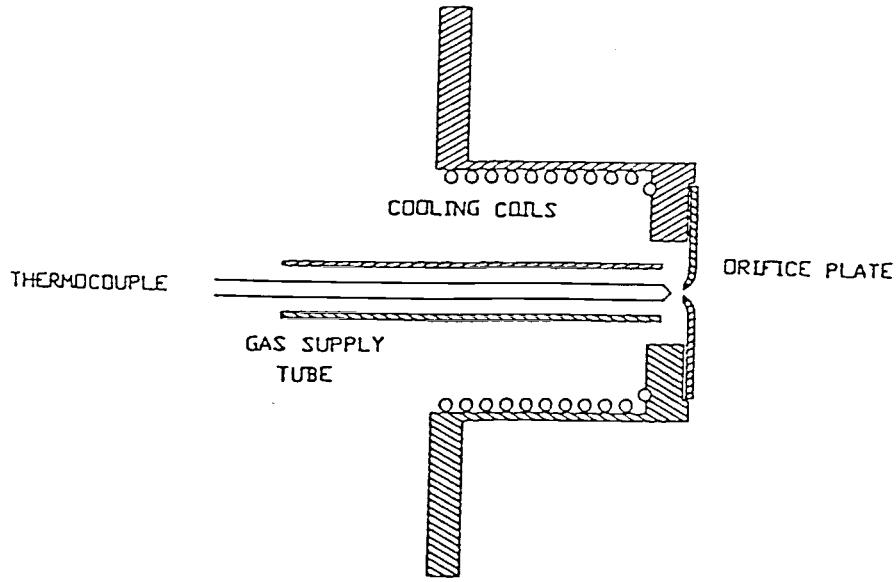

A

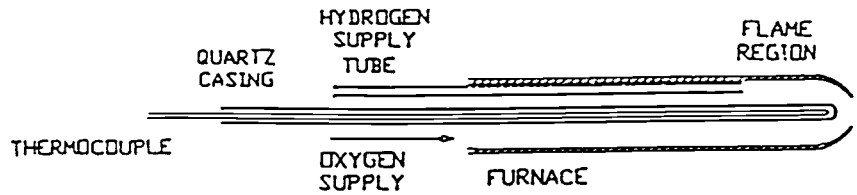

B

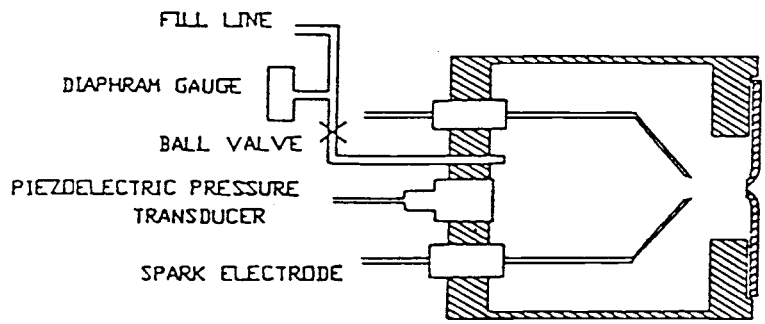

C

Fig. 4 Diagram of various source arrangements. (a) Insert with inner tube for high temperature sampling. (b) Burner for sampling from lean combustion. (c) Combustion chamber for transient experiments.

Steady state spectra of the products of hydrogen/oxygen combustion were recorded using the furnace shown in Fig. 4b. For these measurements, the insert shown in Fig. 4a was placed in the front access port of the vacuum chamber, and the furnace was used as the gas delivery apparatus. The furnace was constructed from quartz, and temperatures near the exit were measured with a quartz-sheathed platnium/rhodium thermocouple. Sampling was performed at atmospheric pressure.

To record each of these spectra, fluorescent emissions from inside the vacuum chamber were collected through a UV grade quality, synthetic fused silica window in the viewing port of the chamber. The emissions were then focused onto the entrance slit of an Acton Research, model VM-505, scanning monochromator having a bandpass (as adjusted by the slit width) of approximately 0.5 nm, and a focal length of 0.5 m. Signal detection was accomplished using a Hamamatsu R955 photomultiplier tube (PMT).

To provide the best possible spectra during these measurements, phase sensitive detection was employed, as is shown in Fig. 5. Signal chopping at 103 Hz was performed by applying a -100 to 0-V square wave to the filament of the electron gun. A Stanford Research model

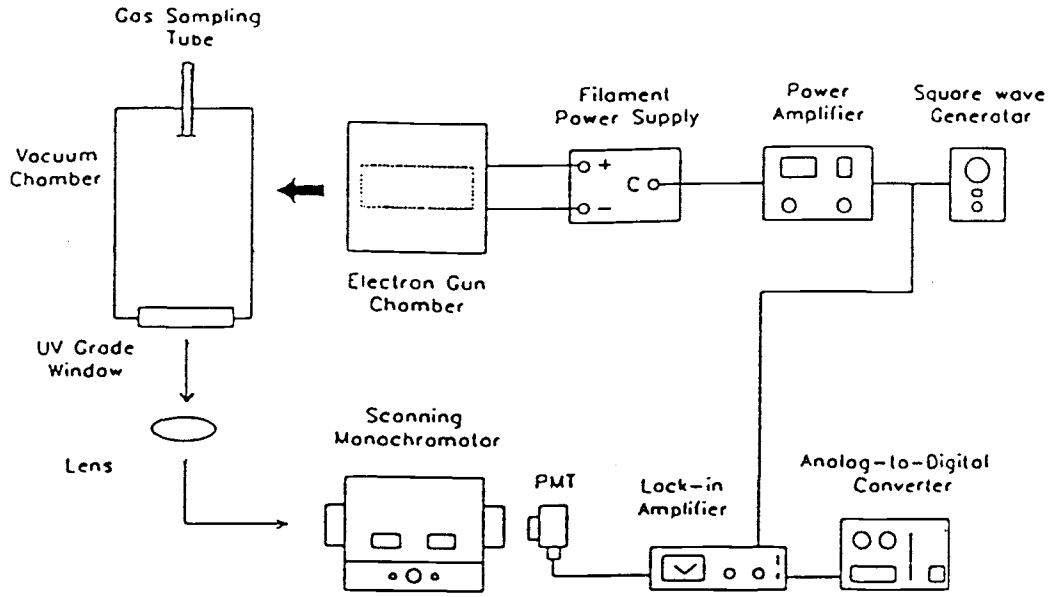

(a) Instrumentation for steady state measurements.

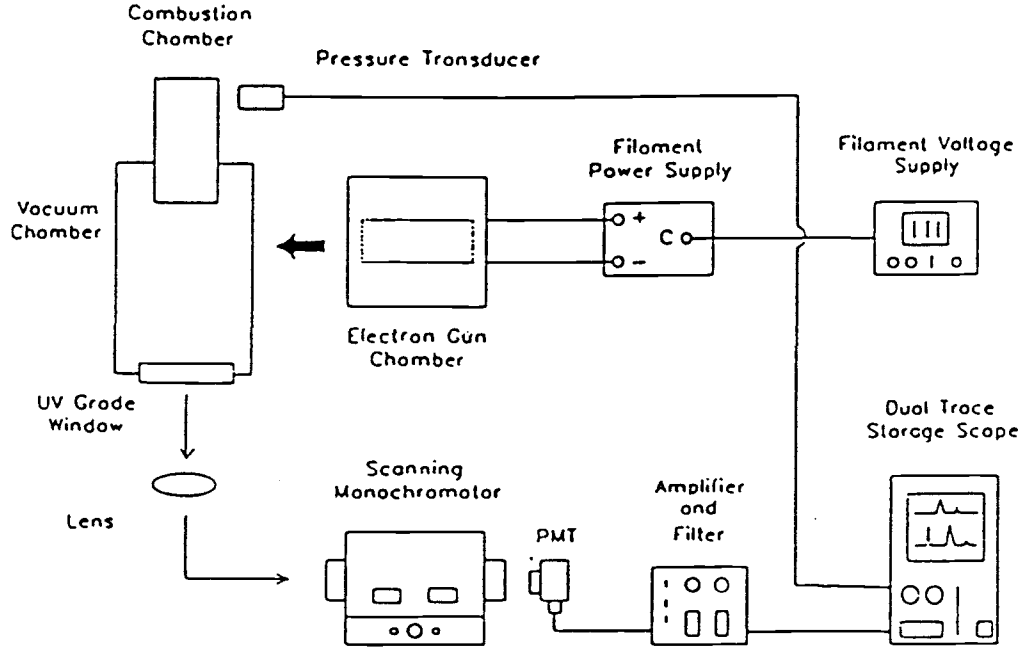

(b) Instrumentation for transient measurements.

Fig. 5 Schematic diagrams of experimental setup.

5102 lock-in amplifier provided phase sensitive discrimination from noise and background, resulting in a signal with a greatly enhanced signal-to-noise ratio. A typical low-pass filter time-constant used when recording the data was 1 second, while the monochromator was scanned at a rate of 5.0 nm/min.

Time resolved detection of nitrogen, oxygen, and water during combustion was accomplished using the source configuration shown in Fig. 4c. The insert was modified by incorporating a closed reaction chamber into the design, with the sampling orifice positioned in one end of the chamber. Interior dimensions of the chamber were 3.7 cm in length and 3.2 cm in diameter. The chamber was equipped with a pair of electrodes, a mixture fill line, and a piezoelectric pressure transducer. Connected to the fill line was a Validyne DP 15-44 diaphragm gauge to measure the initial chamber pressure to within 250 Pa (2 Torr). To begin each combustion experiment, an electrical discharge was initiated between two electrodes positioned approximately 1.1 cm from the sampling orifice. During the experiments, the chamber was isolated from the fill line by a ball valve. The chamber pressure was monitored by a Kistler model 211B5 pressure transducer. All

combustible mixtures were prepared 24 hours in advance, and convective stirring of the mixture ensured a uniform reactant supply for the experiments.

Instrumentation for recording the transient signals differed from that used in the steady-state experiments, as shown in Fig. 5b. For time resolved measurements, a steady -130-V potential was applied to the filament of the electron gun. A higher potential was employed than that used in earlier experiments to achieve higher fluorescent intensity (such an increase has no effect on the spectral output (Peterson, 1988)). For increased signal strength, the monochromator slit width was widened to allow a bandpass of approximately 3 nm. During the experiment, the time dependent PMT signal was first amplified, then conditioned by use of a low-pass filter having a frequency cutoff of 10 kHz, and finally recorded by a Tektronix, model-2230, dual trace, digital oscilloscope having a vertical resolution of eight bits. The sampling rate for all experiments was 500 kHz. The other channel of the scope was used to record the pressure signal during combustion.

3.3 Results and Discussion

3.3.1 REFERENCE SPECTRA

Figure 6 presents spectra for H_2O, N_2, H_2, NO, and

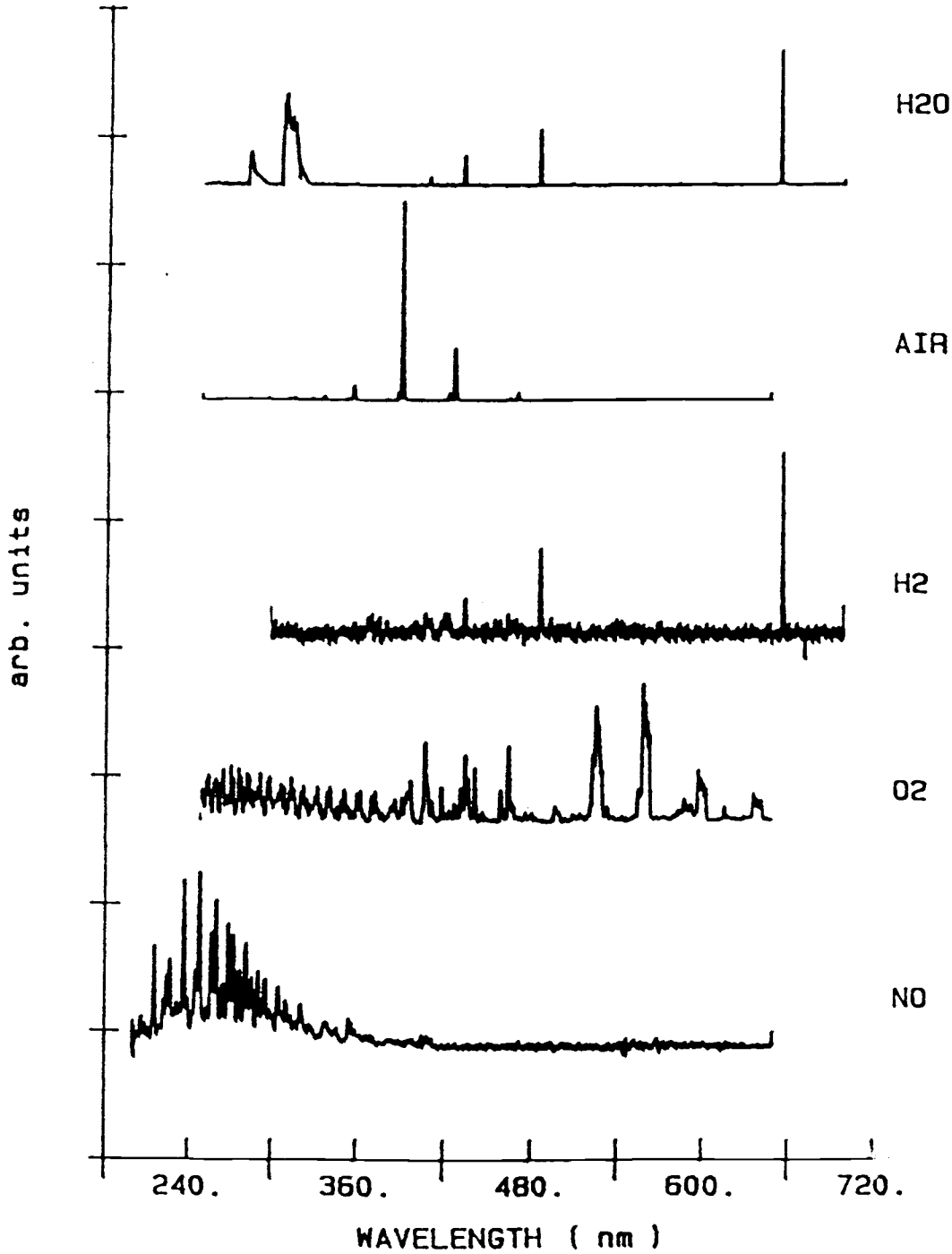

Fig. 6 DSEIF spectra of low temperature gases.

O_2 under steady-state conditions. These curves provided reference spectra for identifying various emission bands in the visible and ultraviolet regions of the spectrum. All curves were recorded under room temperature conditions and a source pressure of one atmosphere, however the amplification factor used in recording each spectrum differed. It should be pointed out that the sampled molecules themselves did not emit detectable radiation, but instead the fluorescing species were ions and radicals created by electron impact. For example, the N_2 spectrum in Fig. 6 comes entirely from the N_2^+ ion, while similarly, oxygen and nitric oxide emission lines originate primarily from O_2^+ and NO^+. The hydrogen atom was responsible for the Balmer line emissions evident in the spectrum of H_2.

The water spectrum was recorded at a source temperature of 575 K. Because electron impact produces excited H and OH radicals, the Balmer lines are present in this spectrum at 656.3, 486.1, 434.1, and 410.2 nm, as well as the OH band structures around 307 and 283 nm (Becker et al., 1980). No fluorescence from the H_2O^+ ion was observed. For the spectra presented in Fig. 6, lines useful in the study of propagating hydrogen/air flames have been selected, and the electronic transitions responsible for these lines were identified. These

values are shown in Table 2.

The effect of combustion temperatures on the spectra of water and oxygen was investigated. A high temperature mixture of O_2 and H_2O was generated by lean hydrogen/air combustion (the burner is shown in Fig. 4b). In these experiments, the temperature measured by the platnium/rhodium thermocouple indicated 1675 K, which was not corrected for radiation. Sampling of the product gases resulted in the electron impact spectrum shown in Fig. 7. The only contrasting feature between this spectrum and the individual ones for O_2 and H_2O is the slight broadening of the O_2 lines around 250 nm. Contributions from excited OH are clearly present in the spectrum, as are the transitions due to O_2^+ between 480 and 600 nm.

The spectra shown in Figs. 6 and 7 exhibit very simple band structures when compared to previously published EIF spectra (Muntz, 1968). The relatively small number of well defined peaks is primarily due to the low temperatures and rarified densities achieved in the free jet. It should be emphasized that the low noise levels achieved in these spectra are a result of using a lock-in amplifier. Fluorescence measurements during transient experiments will display high frequency fluctuations due to shot noise from the PMT.

TABLE 2

Emission Lines Used in the Analysis of Propagating Flames

Parent Molecule	Emitting Species	Wavelength	Transition	Relative Intensity
N_2	N_2^+	391.1 nm	(0,0) First Negitive	120
H_2O	OH	307.5 nm	(0,0) 306.5 nm Band	5
O_2	O_2^+	307.5 nm	(2,4) Second Negative	1
O_2	O_2^+	559.7 nm	(2,1) First Negative	6

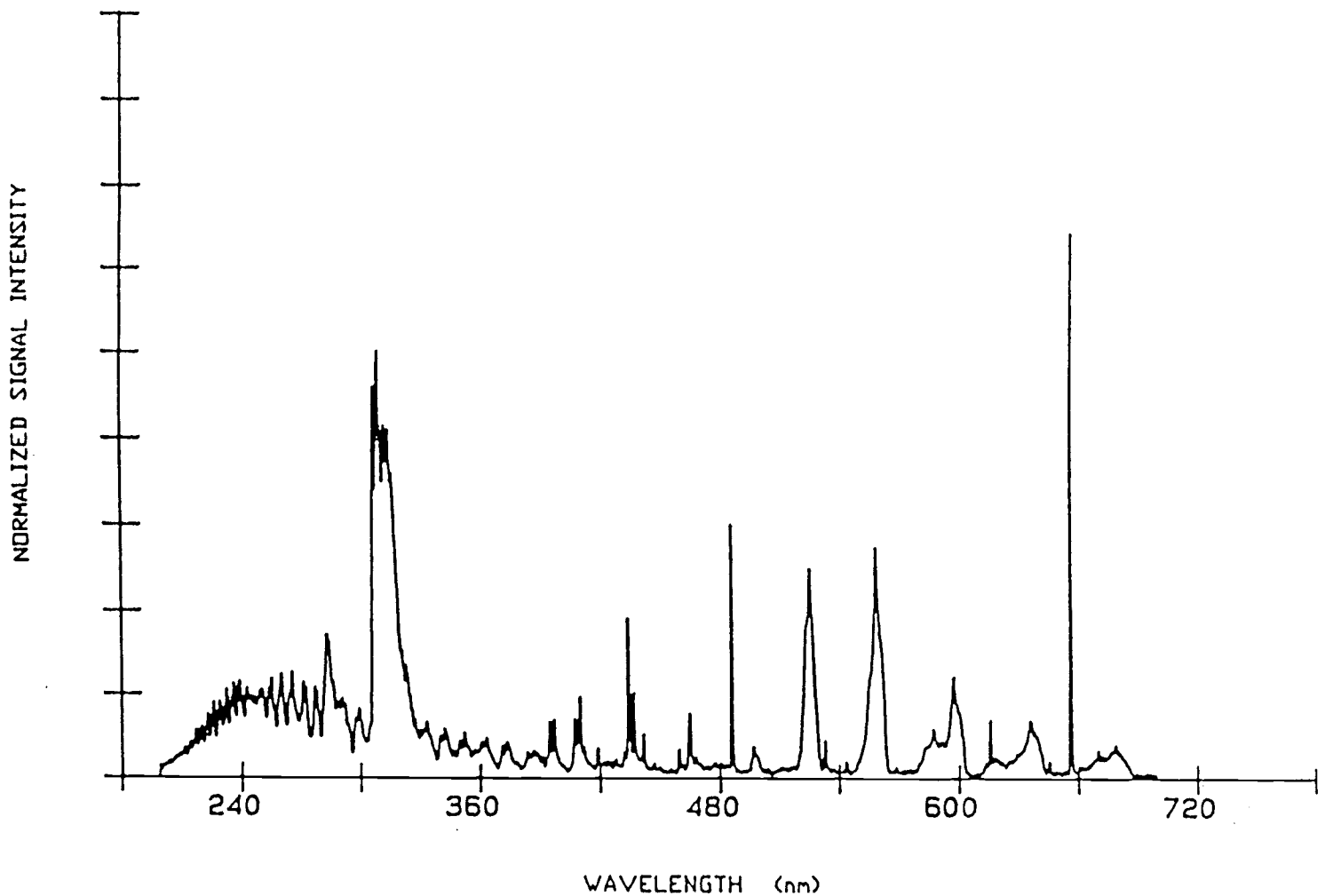

Fig. 7 DSEIF spectrum of lean hydrogen/oxygen combustion.

3.3.2 PROPAGATING FLAME EXPERIMENTS

A propagating hydrogen/air flame was studied using the DSEIF technique to analyze the time-resolved variations in mole fractions during combustion. Experiments were conducted by first filling the chamber to a pressure of 27.6 kPa (200 Torr) with a stoichiometric mixture of hydrogen and air, after which ignition was accomplished by discharging a spark across the electrodes within the chamber. Data from several runs were recorded at wavelengths characteristic of the species under study. Conditions for all runs were kept as close to identical as possible.

Chamber pressure was recorded during each run by the piezoelectric pressure transducer located in the endplate of the chamber. A typical curve is shown in Fig. 8. It displays an increase in pressure due to flame propagation through the mixture, as is characteristic of constant volume combustion. Peak pressures approach those predicted for adiabatic combustion, which is expected since the duration of the event was short($\approx$1.35 ms). The drop in chamber pressure after the maximum value is attributable to temperature induced decalibration of the pressure transducer as well as heat transfer to the chamber walls. During the first

millisecond of the event, decalibration did not occur because the hot gases behind the flame front had not yet come in contact with the transducer.

A typical time dependent fluorescence signal for N_2^+ recorded at 391.1 nm is shown in Fig. 9a. The emission was of sufficient strength to obtain high-quality intensity histories from single experimental runs. At time zero, the mixture was ignited, and the emission intensity increased for approximately 0.8 msec due to the compression of the unburned mixture ahead of the propagating flame. The sharp decrease in emission intensity at 0.9 msec is due to a drop in density at the orifice caused by the arrival of the flame front. This is a result of the high temperature gases behind the flame front moving into the sampling region. After flame arrival, the signal again increases because of the rise in pressure which was induced by continuing flame propagation through other regions of the chamber.

Once the signal was detected by the PMT, filtering was employed to reduce high frequency noise. The highest acceptable time-constant was determined by repeating the experiment a number of times while increasing the time-constant from 0.01 msec to 1.0 msec, and observing the effect on the recorded signal. It was discovered

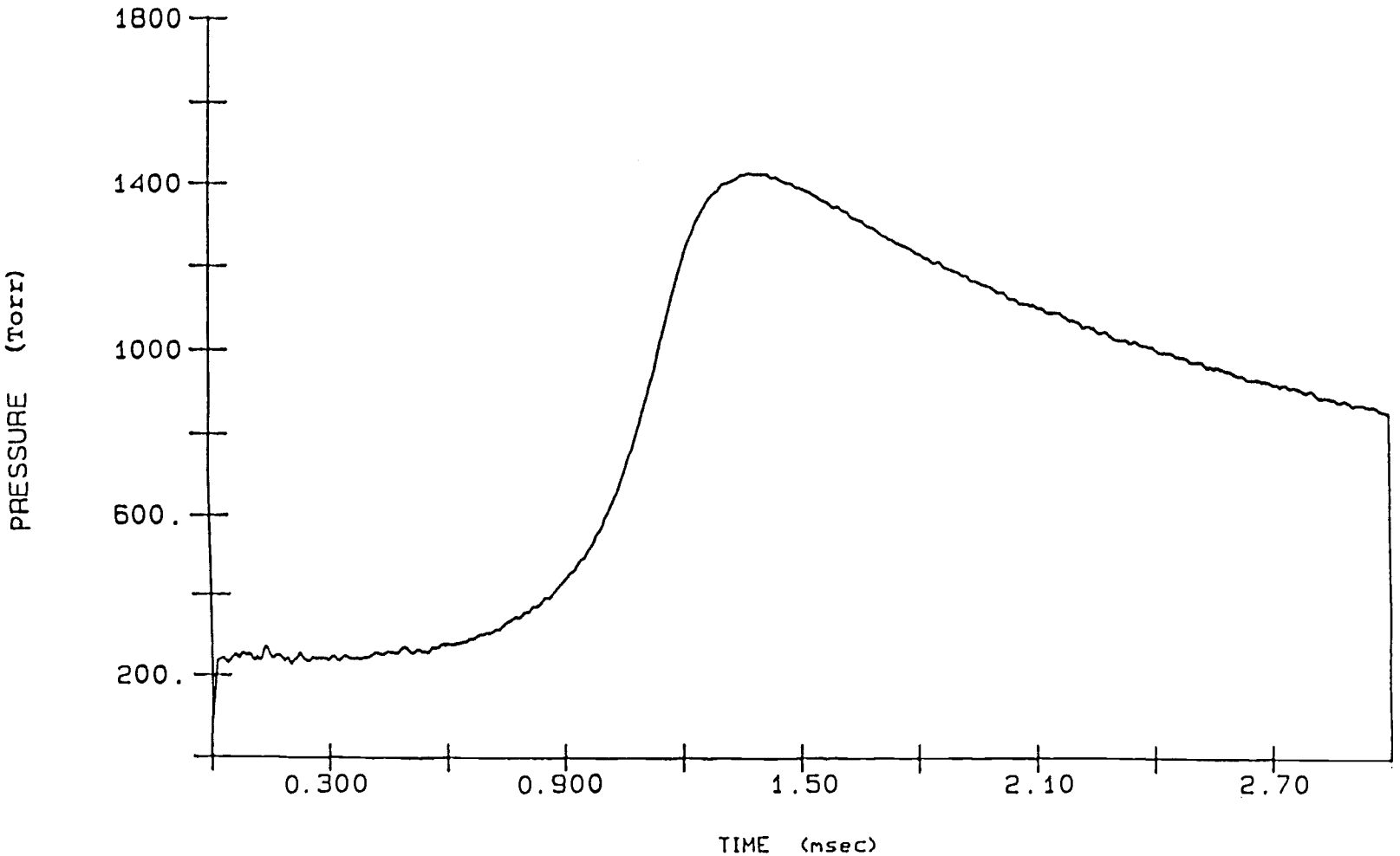

Fig. 8 Combustion chamber pressure during transient combustion.

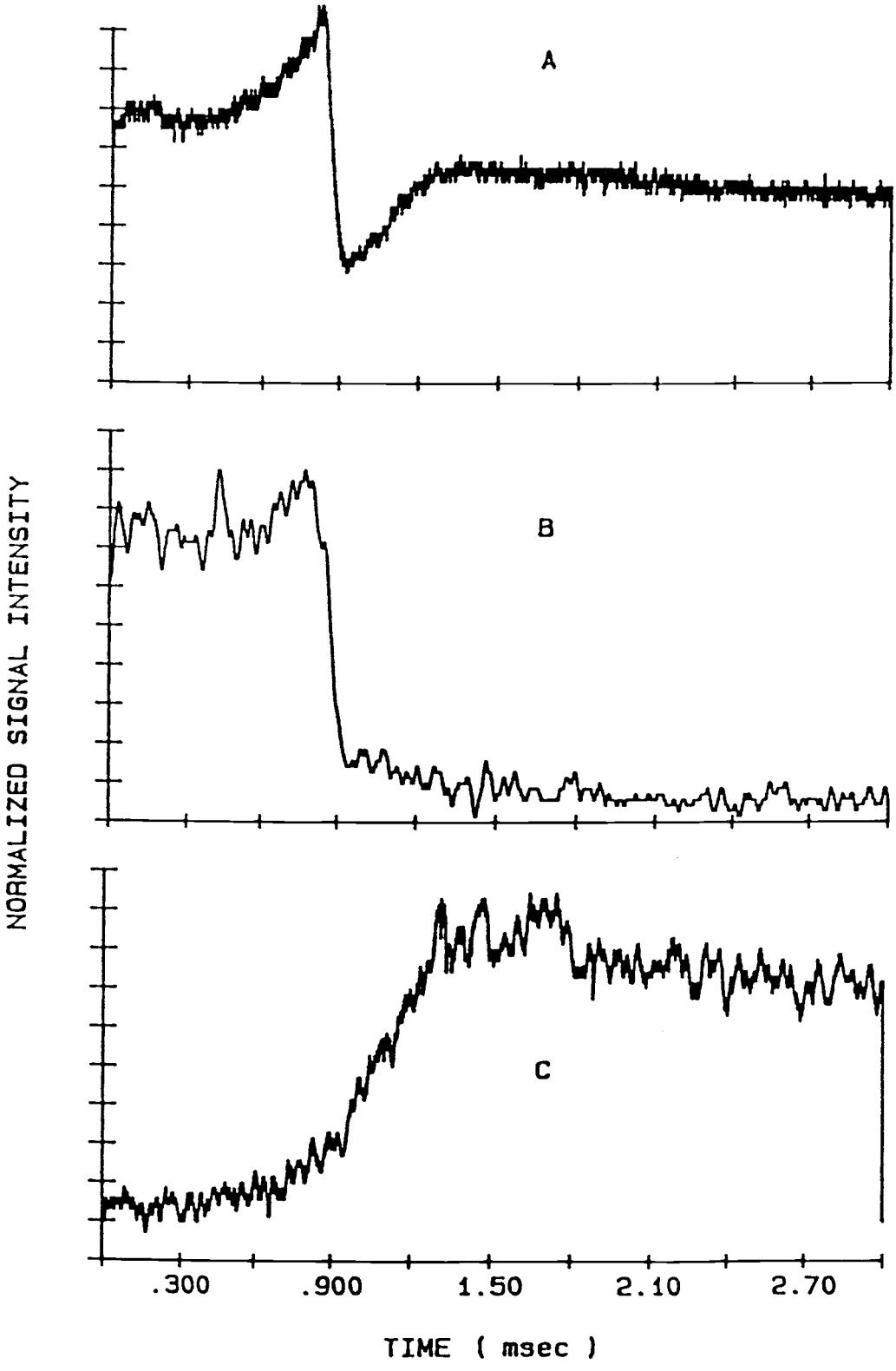

Fig. 9 Emission intensity versus time. Curve (a) was recorded at 391.1 nm, curve (b) at 559.7 nm, and curve (c) at 307.5 nm.

that no significant change in the rise time of the signal occurred with time-constants less than 0.1 msec. This value yielded a reasonable degree of noise rejection, while still preserving the essential time behavior of the signal.

To determine the degree of reproducibility, emissions at 391.1 nm for nine separate experimental runs were recorded under nominally identical conditions. The reproducibility of the experiments was confirmed by the fact that the arrival time at the orifice varied by less than 20 μs for all runs. Signal averaging was therefore a valid method for noise reduction when dealing with low signal-to-noise ratio time histories.

Figure 9b shows the results of averaging the 559.7 nm, O_2^+ emission line intensity during combustion over 16 runs. Averaging was needed because the signal strength was approximately 20 times lower than that recorded for N_2^+. The curve displays a sharp drop at 0.9 ms, as would be expected due to the drop in density and the consumption of O_2 accompanying the arrival of the flame front.

Detection of H_2O was accomplished by recording the fluorescence at 307.5 nm, as is shown in Fig 9c. This curve is the result of signal averaging 12 experimental runs, followed by numerical filtering to remove high

frequency noise. The species responsible for emission at this wavelength are; excited OH formed by fragmentation of H_2O, and O_2^+ formed from O_2. To obtain emissions from OH, the O_2^+ contribution was numerically removed. This was performed by measuring the intensity of the O_2^+ curve obtained at 559.7 nm, scaling this intensity to the level expected from O_2^+ at 307.5 nm, then subtracting this value from that presented in Fig. 9c.

It should be noted that a low level of emissions from electron excitation of flame-generated OH may occur, however no attempt was made to estimate these contributions since electron impact cross-section data for the corresponding transition are not available. In any case, the level of such emissions was much lower than that produced by electron impact dissociation of water.

3.3.3 MOLE FRACTION VARIATIONS

Variations in mole fractions with time for N_2, O_2, and H_2O were obtained by assuming the concentration of minor species was small and that the mole fractions of the reactants were N_2:58%, O_2:14%, and H_2:28%, while those for the products were N_2:65% and H_2O:35%. The N_2^+ emission intensity was then used as a measure of density changes in the jet. The resulting time histories of O_2

and H_2O mole fractions in the jet are presented in Fig. 10. It is important to note that this analysis is based on the assumption that the initial and final mole fractions are known, and it therefore does not provide an absolute measure of mole fractions. Absolute mole fractions might be obtained by creating a region of the jet in which the temperature and pressure are known (a method for producing such a region is described in the following chapter), then recording EIF measurements from this region. Since the absolute number density would be known from pressure and temperature data, the time varying fluorescence could then provide mole fractions if the electron impact cross-section of each species were known.

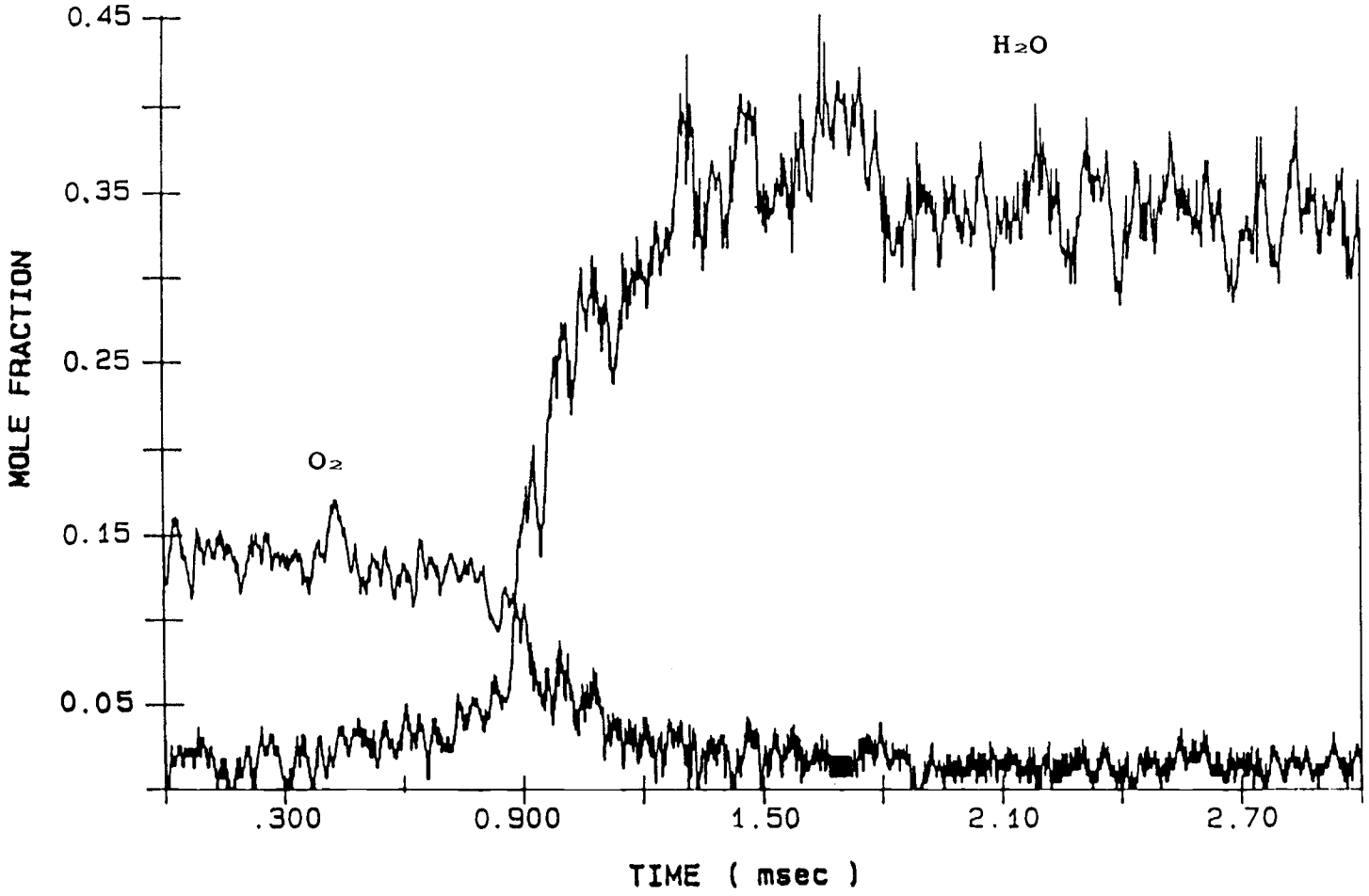

Fig. 10 Time variations of O_2 and H_2O mole fractions.

Chapter 4: MEASUREMENT OF TEMPERATURES AND ATOMIC FREE RADICALS

4.1 Atomic Resonance Absorption Spectroscopy

The second method employed to analyze gas issuing from the sampling orifice was atomic resonance absorption. Measurements using this technique take advantage of the preferential absorption of radiation by atomic species at frequencies corresponding to the energies of their allowed electronic transitions. This effect causes the absorption cross-section of atoms at resonance to be several orders of magnitude greater than that at other frequencies. Therefore, in low density gases, non-resonant absorption may be neglected, allowing absorption at resonant frequencies to provide a method for the detection of atomic species.

A significant limitation of the technique, however, is the necessity of avoiding non-resonant absorption by maintaining low sample density. This limitation is especially stringent in the study of combustion-generated atomic free radicals (such as H, O, or N atoms), since their resonant frequencies are in the vacuum-ultraviolet region of the spectrum. In most typical combustion systems, O_2 and H_2O are in sufficiently high concentrations to totally absorb

radiation at these frequencies. Furthermore, due to the strength of absorption at resonance, the desired target species exist in concentrations that lead to total absorption when experiments are conducted near atmospheric pressure.

These considerations dictate the need to combine resonant absorption with another technique to lower the overall sample density. To accomplish this, direct sampling is used. In this technique, density is reduced to the point where vacuum-ultraviolet radiation can pass through the rarified sample at a specified location downstream from the orifice. By recording the level of resonant absorption during a transient event, it is possible through an appropriate analysis to determine both sample temperatures and concentrations of atomic radicals.

The application of resonant absorption as a diagnostic technique is complicated, however, by the extremely narrow frequency width of resonance lines. This is a problem since, when making absorption measurements, an instrument for resolving frequencies (a monochromator or a filter) must be used. Unfortunately, the bandpass of such instruments is much broader than the frequency width of typical resonance lines. Thus, if radiation is emitted from a continuum source, the

detector will record over a broader frequency range than that in which absorption occurs. This means that, even if atomic species exist in concentrations leading to total absorption of resonant radiation, little decrease in the radiation intensity will be recorded.

To overcome this problem, a radiation source is employed which emits radiation only at resonant frequencies. For studies of combustion-generated free radicals, lamps with this characteristic can be produced by filling a cavity with a gas containing the species of interest, then exciting the gas with microwave radiation. As was the case with EIF, this input of energy creates free radicals with excited electrons, which in turn produce resonant emissions as they fall back to lower energy levels. These emissions may be passed through the sample, thus allowing absorption measurements to be recorded.

The derivation of concentrations and temperatures from such measurements is complicated, however, by: 1) intensity variations with frequency in the lamp emissions, and 2) the frequency dependence of the sample absorption. As a result, a simple application of Beer's law cannot be used to calculate concentrations. In spite of this difficulty, several studies have been conducted in which free radical concentrations have been obtained.

Myerson and Watt (1968) and Thielen and Roth (1987) obtained radical concentrations in shock tube experiments, while Morse and Kaufman (1965) and Michael and Weston (1966) measured radicals in flow reactors. These studies used a direct calibration technique to convert absorption measurements to concentrations. That is, the absorption by gases with known radical concentrations were measured, thus providing a calibration curve. Unknown concentrations could then be determined using this curve and the sample's measured absorption.

This technique is not practical, however, for studies of transient combustion processes. Due to the thermal dependence of Doppler effects, the frequency profile of sample absorption changes with temperature. As a result, any calibration curve is only valid for a single sample temperature. To overcome this limitation, a mathematical model of the both the lamp emissions and the sample absorption may be developed. The advantage of such a model is it allows both local temperatures and radical concentrations to be calculated from absorption measurements.

The technique used to obtain sample temperatures during transient events relies on the addition of a small fraction of an inert gas to the combustible

mixture. This provides an atomic species with a known concentration throughout the combustion event so that measurements of resonant absorption by the species permit temperatures to be derived. In this study the inert gas used was krypton (krypton was selected since it has a resonant line very near the hydrogen Lyman-α line). A small percentage of krypton is sufficient to provide high levels of resonant absorption, while the concomitant effects on the fluid and thermodynamic characteristics of the sample are negligible.

4.2 Development of Mathematical Model

4.2.1 ATOMIC RESONANCE LAMPS

A number of researchers have studied the spectral output of atomic resonance lamps (Braun and Carrington, 1969; Braun, 1970; Lifshitz et al., 1979; Maki et al., 1985). In each of these investigations, high resolution monochromators were used to record spectra of resonant emissions from hydrogen atoms. Hydrogen emissions are especially well suited to such studies since they have the broadest frequency width of all atomic resonant lines, therefore allowing the best spectral resolution.

The spectra recorded in each study, however, were distorted due to the instrument functions of the monochromators. Such distortions were accounted for by

the development of mathematical models of the emissions, which allowed numerical corrections for the instrument functions to be performed. Conclusions from these investigations can be summarized as:

* The primary factor governing the frequency width of a resonant line is Doppler broadening. This occurs due to the thermal motion of the emitting atoms. Lorentz broadening may be neglected due to the low pressures maintained in resonance lamps.
* Resonant emissions from a lamp do not have the Gaussian profile which would be expected from a thermal speed distribution. This occurs because, before the radiation can exit the lamp, it is attenuated due to absorption by the same species that generate the radiation - an effect that is termed "self-absorption". This process selectively absorbs radiation from the center of the resonance line, creating an emission line profile with a local minimum at the center and maxima at the wings.
* The degree of self-absorption depends on both the concentration of the emitting species in the lamp and the depth of the emitting region. The lowest self-absorption occurred when lamps were operated with small hydrogen atom concentrations and thin emitting regions.

* Temperature variations existed within the lamps. In all experiments, the emitting gas was in contact with a UV-transparent window. Temperatures were highest near the center of the emitting region due to the input of microwave energy, and were lowest near the window and cavity walls due to heat transfer.
* Mathematical models taking into account instrument function distortions have been successful in predicting the shape of resonant lines. These models are based on the assumption that the lamp can be treated as an isothermal emitting and absorbing region, followed by an absorbing region at a lower temperature. The second absorbing region accounts for the cooler region near the window.
* Calibrations of the instrument function of a particular monochromator can be obtained by scanning the resonant lines emitted from heavy atoms such as Hg or Kr. These lines are so narrow that, even at highest resolution, their recorded profiles are a good approximation of the instrument function.

In the current study, a lamp was constructed which employed opposing jets of an emitter and helium. This design produced an optical emission zone which did not come in contact with the lamp window (a description of

this lamp is found in the experimental section). Due to the thin, nearly isothermal, emission-absorption zone, it is assumed the lamp can be modeled as an emitting region followed by an absorbing region at a uniform temperature. This means, for a singlet resonance line, a thermal speed distribution predicts that, before self-absorption, emissions will have a Gaussian profile due to Doppler broadening, with the width at one half maximum given by; (Boiteux, 1965)

$$\Delta\nu_D = \nu_0 \sqrt{\frac{8kT\ln(2)}{mc^2}} \tag{5}$$

where ν_0 is the frequency at the center of the emission band, k is Boltzmann's constant, T is the temperature of the gas, m is the atomic mass, and c is the speed of light.

To quantify the effect of self-absorption on this profile, Beer's law can be applied to each portion of the emission line, allowing the resulting profile to be written as;

$$I(\nu) = I_D(\nu) \times \exp[-K(\nu)\,l] \tag{6}$$

where l is the length of the absorbing region, the emitting region's doppler profile, $I_D(\nu)$, is given by;

$$I_D(\nu) = I_D(\nu_0)\exp\left[-\left(\frac{\nu-\nu_0}{0.6\Delta\nu_D}\right)^2\right] \tag{7}$$

and the function $K(\nu)$ accounts for the wavelength dependent absorption intensity which is given by;

$$K(\nu) = \left[\frac{1}{l}\ln\left(\frac{I(\nu_0)}{I_D(\nu_0)}\right)\right] \times \exp\left[-\left(\frac{\nu-\nu_0}{0.6\Delta\nu_D}\right)^2\right] \qquad (8)$$

where $I(\nu_0)/I_D(\nu_0)$ is the transmittance fraction at the center of the emission band. Note that the first quantity in brackets is given the symbol K_0, or the centerline absorption coefficient.

The proposed model of lamp emission (an emitting region followed by an absorbing region) is relatively simple. This is an advantage that allows the frequency profile of a specific resonant line to be characterized by two parameters; the emitter-absorber temperature, T_L, and the lamp centerline absorption coefficient, K_{0L}. The most straightforward way to obtain these two parameters would be to perform a scan of the line with a high resolution monochromator then numerically correct the measured profile to account for distortions introduced by the monochromator instrument function. From the actual line profile, the parameters could then be deduced. The problem with this approach is that most resonant lines are too narrow to be resolved.

For emissions from heavy atoms such as krypton, values of the two characterizing parameters must therefore be obtained indirectly. To estimate the

emission temperature, the lamp may be operated with a gas containing both hydrogen and krypton, and a spectrum recorded of the Lyman-α line. A mathematical fit to the recorded lineshape can be performed using the proposed model, where T_L and K_{0L} are the parameters of variation. Again, lineshape corrections must be made to account for instrument function distortions. Once the lamp emitter temperature has been found, the lamp centerline absorption coefficient for krypton is obtained from sample absorption measurements.

4.2.2 SAMPLE ABSORPTION

To develop a model of the sample absorption, it is necessary to determine unique values for the sample temperature. In a free jet, this is difficult to perform due to the non-uniform speed distribution the gas attains as it expands from the orifice. To avoid this problem, a flow tube similar to a stagnation temperature probe can be positioned downstream from the orifice in the region of hypersonic flow. It has been demonstrated that such probes generate a detached normal shock wave, where the temperature behind the shock approaches the stagnation temperature of the flow (Winkler, 1954; Shadday et al., 1978). If an evacuated optical path is

provided so that resonant absorption occurs only across the diameter of the tube, absorption will then take place in a gas of near uniform temperature and pressure.

The equations describing sample absorption are the same as those for absorption in the lamp. Thus, when a gas sample is extracted from a mixture of known composition and temperature under steady state conditions, the centerline absorption coefficient, K_{0S}, is obtained using the relation (Morse and Kaufman, 1965)

$$K_{0_s} = 2f\left(\frac{\pi}{\ln 2}\right)^{-1/2} \frac{\pi e^2}{mc} \frac{n}{\Delta\nu_D} \qquad (9)$$

In this relationship, f is the transition oscillator strength, n is the krypton number density in the flow tube, and $\Delta\nu_D$ is the doppler half-width of the sample's absorption line. The value of f is obtained from the literature, while $\Delta\nu_D$ and n are obtained from the known values of the sample temperature, the krypton mole fraction, and from measurements of the pressure in the flow tube.

Using these sample absorption characteristics, a summarized procedure for determining K_{0L} is as follows:

* $K(\nu)$ of the sampled gas in the flow tube is calculated from known quantities.

* A trial $I_D(\nu)$ for the lamp is determined using the temperature found earlier (from the hydrogen line emission) and an assumed value of K_{0L}.
* A trial theoretical absorption value is obtained by solving for the intensity profile after sample absorption by using the known $K(\nu)$ and the assumed K_{0L}, then integrating the resulting profile.
* The procedure is repeated using refined estimates of K_{0L} until the integrated theoretical absorption corresponds to the experimentally measured value.

4.2.3 SAMPLE TEMPERATURES

After K_{0L} is obtained for krypton emissions, unknown sample temperatures can be determined by first finding a K_{0S} value for which the measured and predicted absorption values match, then finding a sample temperature which would produce the K_{0S}.

This procedure for determining temperatures may appear involved, however it is based on relatively few assumptions. The validity of the model can also be checked by comparing experimentally measured temperatures with those predicted numerically from absorption values. This is demonstrated in a later section.

4.2.4 ATOMIC HYDROGEN CONCENTRATIONS

Once the sample temperatures are determined during a transient event, the concentration of hydrogen free radicals may be obtained from measurements of the absorption of Lyman-α radiation. In these experiments, the values of T_L and K_{0L} describing the lamp emission profiles can be derived by the procedure used earlier to provide the lamp emission temperature. An iterative numerical routine is then employed to yield radical concentrations. The steps in this analysis are as follows:

* An initial estimate of K_{0S} is made (based on known sample temperature, assumed number density, and literature values for other quantities).
* The transmitted line profile, $I(\nu)$, is calculated using the estimated value of K_{0S}.
* $I(\nu)$ is integrated and compared to the experimentally measured line intensity after sample absorption.
* The procedure is repeated with refined values of n until calculated and measured absorption values agree. This gives the hydrogen atom number density at one time point in the recorded transient absorption curve.

A fortran code written to perform these calculations, is listed in Appendix 1.

4.2.5 RESONANCE OF ATOMIC SPECIES

When applying this technique, it is important to note that essentially all of the atoms in the sample will be in their lowest electronic state. As a result, the only resonant radiation which will be significantly absorbed is that associated with ground state transitions. Table 3 presents frequencies, transitions, and oscillator strengths for some resonant lines useful in studying combustion-generated atomic radicals.

For the transitions shown in the table, the modeling assumption of a single-valued underlying resonance line was only true for krypton emissions. The hydrogen peaks, however, are so close together that their split was an order of magnitude smaller than the spreading caused by doppler effects. This allowed them to be treated as a singlet. To calculate the equivalent oscillator strength, the two lines were considered to be produced by transitions from two degenerate states. This permitted their values to be summed to yield a strength of 0.832 (Morse and Kaufman, 1965).

On the other hand, the separation between triplet lines for O and N radiation is large enough that Doppler

Table 3

Resonant Lines Useful in Studying Combustion-Generated Free Radicals

Species	Frequency (cm^{-1})	(Wavelength) nm	Transition	Oscillator Strength
Kr	80919	123.58	$(4P^5 5S)^2P_{3/2} \rightarrow (4P^6)^1S_o$	0.16
H	82281.3	121.53	$(2P)^2P_{1/2} \rightarrow (1S)^2S_{1/2}$	0.555
	82281.6	121.53		0.277
N	83361	119.96	$(2P^2 3S)^4P \rightarrow (2P^3)^4S^o$	0.71
	83319	120.02		0.47
	83285	120.07		0.24
O	76793	130.22	$(2P^3 3S)^3S_1^o \rightarrow (2P^4)^3S_2$	0.16
	76634	130.49	$(2P^3 3S)^3S_1^o \rightarrow (2P^4)^3S_1$	0.095
	76570	130.60	$(2P^3 3S)^3S_1^o \rightarrow (2P^4)^3S_o$	0.032

Transitions and oscillator strengths are from Wiese et al. (1966), Davis and Braun (1968) and Zaidel (1970).

effects do not cause the lines to overlap. For both triplets, the frequency split between lines is greater than 0.05 nm, while the expected broadening from Doppler effects is on the order of 0.002 nm. Thus, each peak of the triplets may be modeled individually.

Two complications, however, arise with this analysis. The first is that resonant lines from O and N atoms are too narrow to be spectrally resolved with a monochromator. This means an alternate method of determining the frequency profile of each peak is needed.

The second complication is that, for practical measurements of transient events, the bandpass of the monochromator must be wider than the separation between peaks. This means that the three lines of each triplet will be recorded simultaneously.

To account for these effects, the following observations can be made:

* Before self-absorption, the intensity of emissions from the lines of a triplet will be proportional to their oscillator strengths. In addition, the effects of Doppler broadening on each line will be identical.
* During self-absorption, the ratio of the absorption coefficients for each line will also be proportional

to the oscillator strengths. Thus the lines with the strongest emissions will have the greatest reduction in their total intensity.

* The K_{0L} for each line may then be deduced by either of two techniques. The first is a direct calibration as discussed by Morse and Kaufman (1965), Myerson and Watt (1966), Maki el al. (1985), and Thielen and Roth (1987). The second technique relies on measuring the relative intensities of each line of the triplet. Because the stronger emission lines will be subject to proportionally greater self-absorption, the ratio of the intensities of the lines will depend on the level of self-absorption. Using the model developed in this study, a correlation can be developed yielding the expected strength of each line as a function of the absorption coefficients. In this analysis, it is important to note that the ratio of the K_{0L} values for each line remain constant. Thus, if the lamp emission temperature is known, the ratio of the observed triplet line intensities can yield the self-absorption values.

* Once the lamp characteristics are determined, concentrations of O and N atoms in the sample can be deduced from absorption measurements. This analysis

is similar to that for hydrogen, except, in this case, three lines must be treated simultaneously. To do this, the relative strengths of the three emission lines are recorded, and the overall absorption fraction in each line is calculated using a range of K_{0S} values. Again, the calculations must be performed in sets of three with the ratio of K_{0S} values matching the ratio of the oscillator strengths. The total absorption over all three lines for each set of calculations is then obtained by summing the intensities of the three lines before and after sample absorption. An estimate of the sample concentration may then be derived from the K_{0S} values for which predicted and experimentally measured absorption levels are equal.

4.3 Experimental

The Direct Sampling Atomic Resonance Absorption Spectroscopy (DSARAS) apparatus used in this investigation is shown in Fig. 11. The vacuum chamber and pumping arrangement was identical to that used in DSEIF experiments, however, for this study, the two side ports contained a microwave discharge lamp and an aperture having a diameter of 1.5 mm. The aperture was connected through an evacuated tube to the entrance of a monochromator. The front panel contained either the

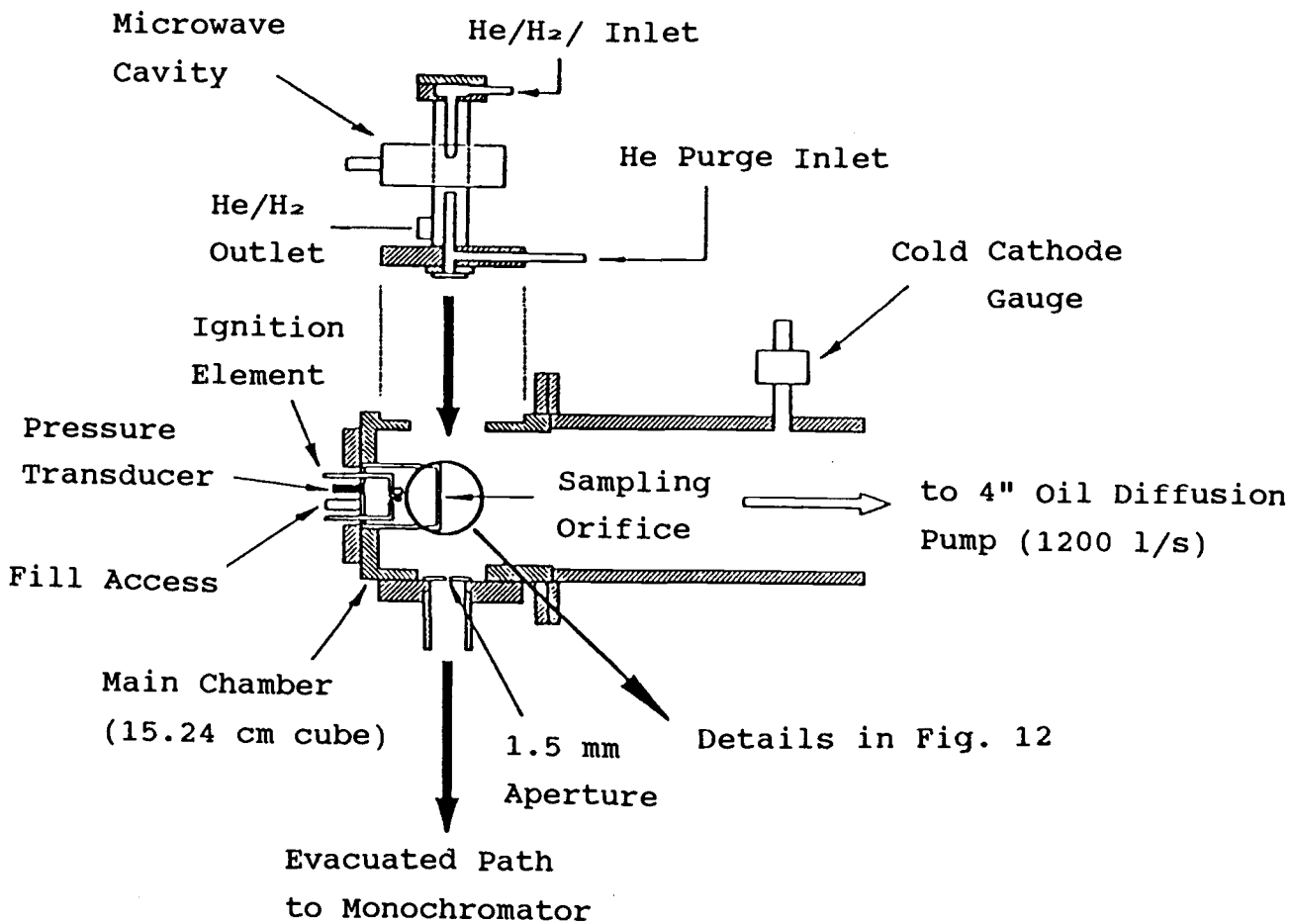

Fig. 11 Diagnostic portion of Direct Sampling Atomic Resonance Absorption Spectroscopy (DSARAS) apparatus.

combustion cell, as pictured in Fig. 11, or a steady state gas delivery apparatus, similar to that used in obtaining H_2O spectra in DSEIF experiments.

The combustion cell was a cylindrical vessel 5.1 cm in length and 3.2 cm in diameter, which was equipped with a coiled nichrome ignition element, a fill line, and a piezoelectric pressure transducer. Connected to the fill line was a Validyne DP14-44 diaphragm gauge to measure the initial pressure to within 250 Pa (2 torr). Two sampling configurations were used; the first being a 0.20-mm orifice in the center of a brass foil endplate, and the second being a 0.18-mm conical orifice in the apex of a hollow quartz cone fixed to the chamber endplate. The cone projected 2 mm into the chamber and had an interior angle of 70 degrees an exterior angle of 110 degrees, and an estimated channel length of 3 mm.

The steady-state gas delivery apparatus consisted of an insert containing a brass foil endplate with a 0.08-mm sampling orifice. Gas samples were supplied through a 1.0-mm orifice in a quartz tube positioned less than 2 mm from the sampling orifice. The insert was open to the atmosphere, allowing excess gas supplied by the delivery tube to escape into the surroundings. Reproducible delivery rates were obtained by measuring the pressure in the supply tube. High temperature gas

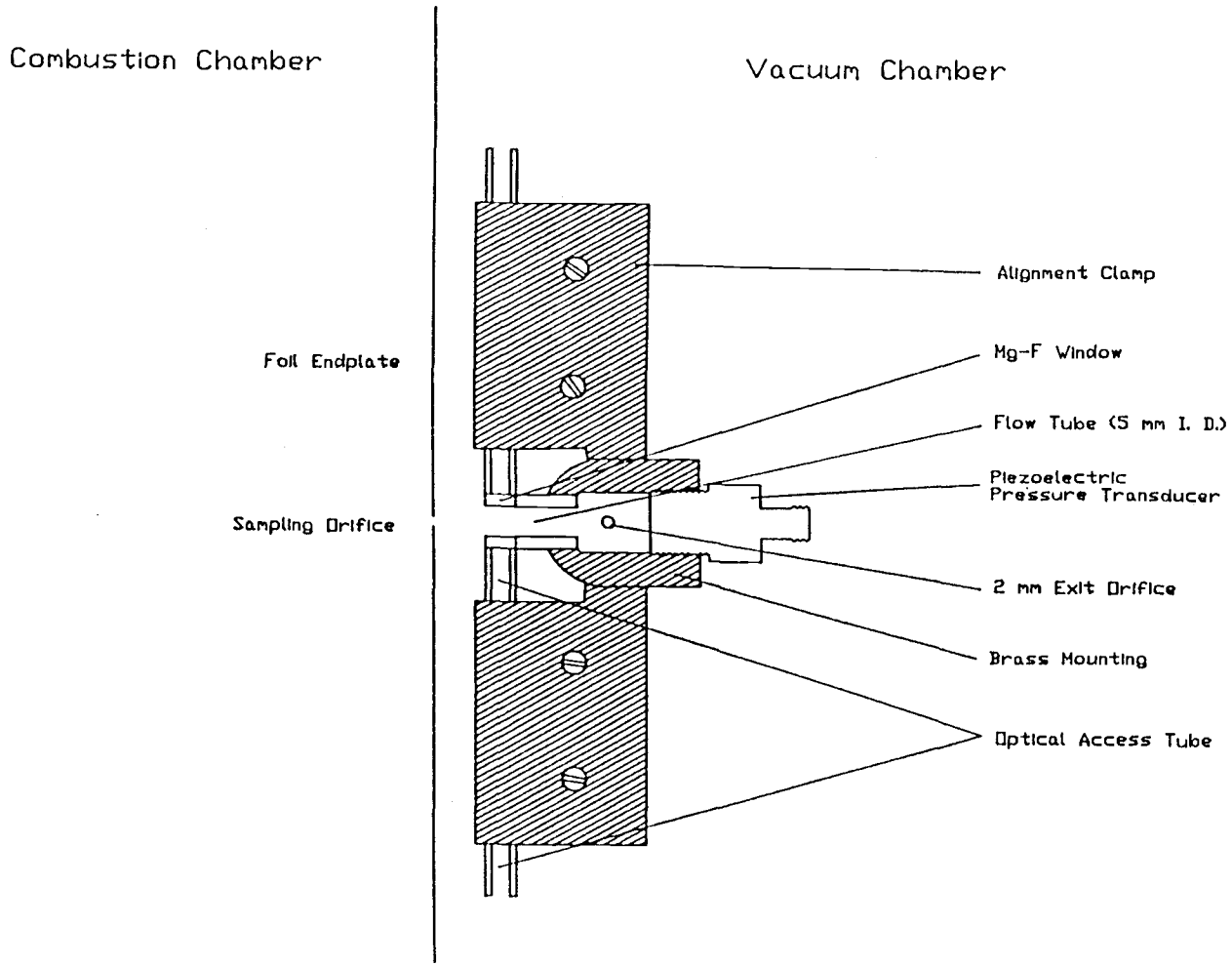

Fig. 12 Flow tube for absorption measurements.

samples were provided by a resistively heated nichrome wire coiled around the tube, and gas temperatures were recorded with a chromel-alumel thermocouple, placed inside the tube near the exit.

A normal shock was generated by a tube positioned in the free jet issuing from the sampling orifice. The apparatus containing this tube is depicted in Fig. 12. The tube had an inner diameter of 0.5 cm, and was located downstream from the orifice along the jet centerline. In experiments using the brass foil sampling arrangement, the distance from the orifice to the inlet of the flow tube was 0.4 cm, and when the cone arrangement was employed, the distance was 0.55 cm. Selection of this distance was provided by use of variable thickness spacers between the combustion chamber and the vacuum chamber. An evacuated path for UV radiation was provided by access tubes mounted perpendicular to the jet centerline at the front of the tube. At the points of intersection, the walls of the quartz tube were ground away, and magnesium fluoride windows 2-mm thick were attached. A distance of 0.46 cm was measured between the faces of the windows. A brass mounting which supported the tube, contained a Kistler 211B5 piezoelectric pressure transducer and a connection (not shown in the figure) leading to a diaphragm gauge.

Static pressures in the tube were measured with a precision of 0.25 Pa ($2x10^{-3}$ Torr), and subsonic flow was produced by a 0.2-cm orifice near the end of the brass support.

To begin each transient experiment, the combustion chamber was filled with a flammable mixture of stoichiometric hydrogen and air. A current of 9.7 amps was passed through the ignition coil, which resulted in initiation of combustion after approximately 4 sec of heating. During each experiment, the chamber pressure was monitored by a Kistler, model 211B3 pressure transducer mounted in the wall opposite the sampling orifice. The sharp rise in pressure due to combustion was used to trigger sampling by a digital oscilloscope. All combustible mixtures were prepared 24 hours in advance in a partial pressure mixing tank, with convective stirring used to ensure a uniform reactant supply.

A schematic diagram of the instrumentation used in this experiment is shown in Fig. 13. The lamp required two gas supplies; one of 5% hydrogen and 5% krypton in a balance of helium, and the other of pure helium. Needle valves in the supply lines and a mechanical vacuum pump on the exhaust line permitted lamp flow rates and pressures to be adjusted. A 100-W microwave power supply

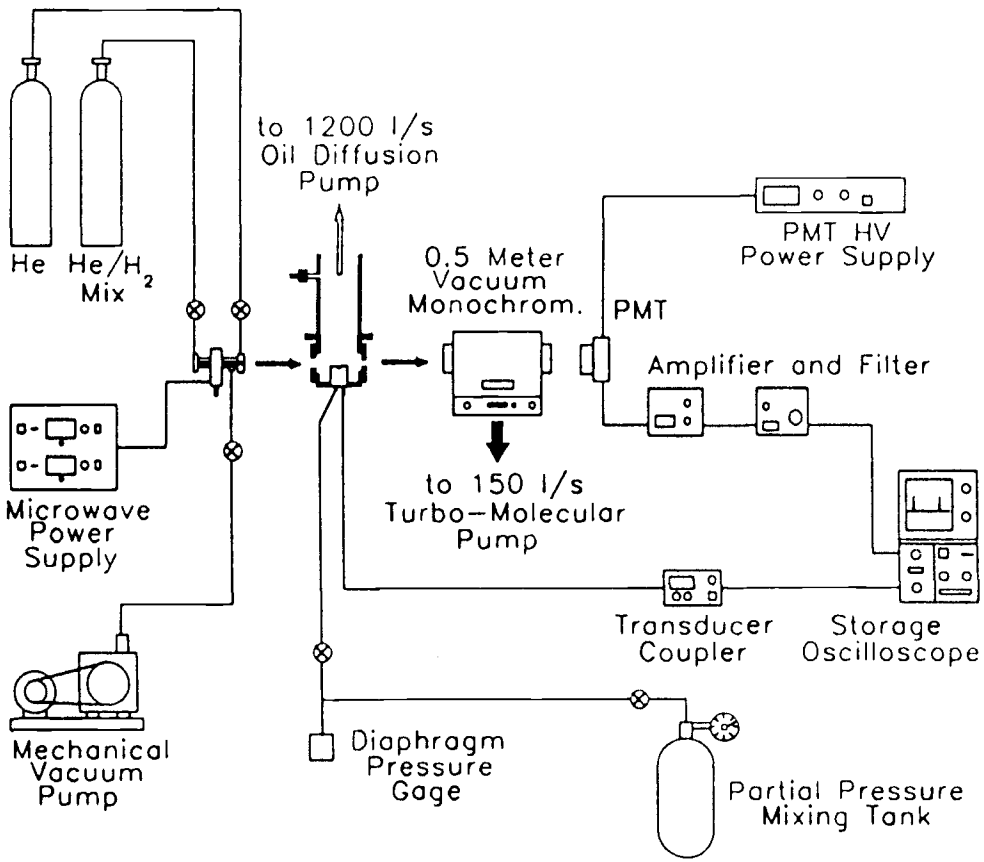

Fig. 13 Schematic diagram of the DSARAS instrumentation.

was connected to an Evanson-type cavity (details of the lamp design are given shortly) that enclosed a section of the lamp discharge tube. The detection side of the apparatus included a 0.5-meter vacuum monochromator connected to the vacuum chamber by an evacuated coupling 25 cm in length. This meant the distance from the monochromator to the lamp and the sample absorption tube was 40 cm and 33 cm respectively. The monochromator employed an Acton Research, 1200 groove/mm, $AlMgF_2$-coated grating which had been blazed for peak efficiency at 250 nm. Pressures below .001 Pa (10^{-5} Torr) were maintained in the monochromator by use of a 150-l/s turbo-molecular pump. Detection of vacuum UV radiation was accomplished with a Hamamatsu R-1259 photomultiplier tube with a Mg-F window. The signal output was first amplified by a wide-band video amplifier, then sent through a low-pass filter having a frequency cutoff of 3 kHz. During each experimental run, the Tektronix digital storage oscilloscope simultaneously recorded both the pressure trace from the combustion chamber, and either the absorption signal or the amplified pressure signal from the piezoelectric pressure transducer mounted in the flow tube. Sampling was performed at a rate of 200 kHz.

A lamp which was specially developed for use in this experiment is shown in Fig. 14. The objective of this development was to construct an emission source with an optically thin emitting region, thus producing high intensity resonance lines with minimal self-absorption. To accomplish this, a cylindrical lamp was designed which employed two opposing gas flows - one flow contained the emitting gas, while the other was comprised of helium. Emissions were then produced in the thin stagnation region formed between the flows. Low pressures in the lamp ($\approx$ 0.3 kPa (2 Torr)) were maintained by pumping with a mechanical vacuum pump.

Design features of the lamp included a 1.5-cm O.D. quartz outer tube which was fitted with a Evanson-type microwave cavity. In addition, to provide the opposing gas flows, two 3-mm O.D. tubes were positioned inside the lamp along the centerline. Flow rates through the tubes were controlled with needle valves. These tubes were mounted in brass fittings on either end of the lamp, and their length was such that a 1-cm gap existed inside the microwave stimulated region. The helium supply tube had no flow restrictions, however the tube supplying the emitter gas terminated in a 120-micrometer orifice. This allowed for the formation of a low mass flow, supersonic, free jet of emitter gas into the lamp.

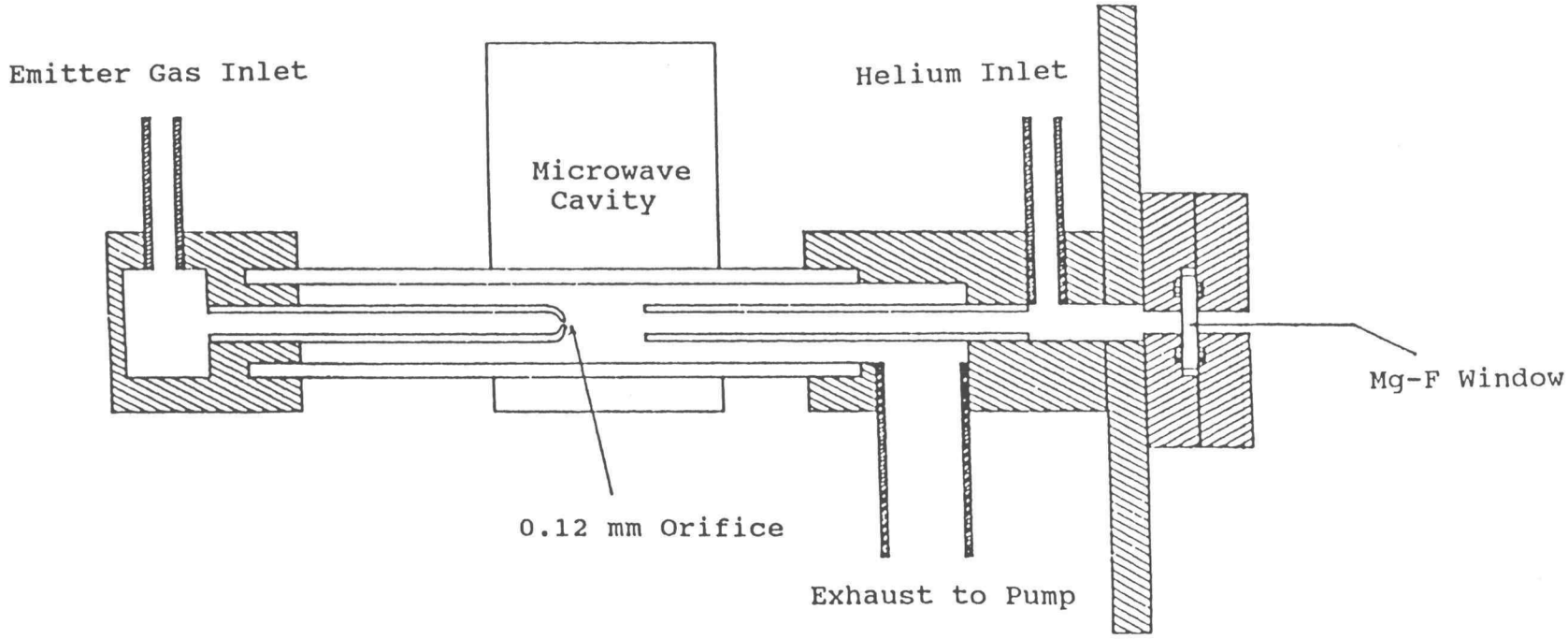

Fig. 14 Atomic resonance lamp.

Helium flow from the opposing tube induced a normal shock in this jet so that, after passing through the shock, the emitting species were swept towards the edges of the lamp. An optical pathway through the length of the helium tube was provided to allow resonant radiation to pass into the vacuum chamber through a 2-mm thick Mg-F window. Most of the radiation was produced within the thin region between the shock and the helium flow. Few emissions were generated in the supersonic jet since the density of that region was relatively low.

4.4 Results and Discussion

4.4.1 LAMP OPERATION

In this study, the resonant frequencies employed were the hydrogen Lyman-α line and the 123.5-nm krypton line. In order to achieve the maximum signal strength for absorption measurements, the monochromator's second-order peak of each line was selected. The reason for employing the second-order lines was that, due to the blaze characteristics of the monochromator grating, the signal strengths detected by the PMT for the first and second-order lines were approximately equal. However, the greater frequency separation between the hydrogen and krypton lines in the second order allowed for a wider bandpass (1.50 mm slit width) to be

selected. Spectra of the second-order krypton and Lyman-α lines at high resolution as well as with a monochromator slit width of 1.50 mm are shown in Fig. 15.

The emitting gas used in this study was comprised of 5% Kr and 5% H_2 in a balance of helium. Pressures in the lamp were primarily dependent on the helium purge flow rate, and maximum signal strengths were produced when the lamp internal pressure was 0.3 kPa (2 Torr). Using this lamp pressure, the Lyman-α signal strength as a function of the emitter gas pressure upstream of the orifice was recorded. A plot of these strengths is shown in Fig. 16. An additional plot presenting the variation of K_{0L} with emitter gas pressures upstream of the orifice for both Kr and H emissions is shown in Fig. 17.

4.4.2 LAMP EMISSION PROFILES

In order to obtain the lamp emission temperature and the lineshape of hydrogen emissions, Lyman-α line profiles were recorded for various H_2/Kr/He lamp flow rates at a lamp power of 30 W. The necessary resolution was achieved by using a 316 gr/mm Eschelle grating in the monochromator. The grating was rotated approximately 60 degrees for operation in the 47th order. Examples of the recorded spectra are shown in Fig. 18, while

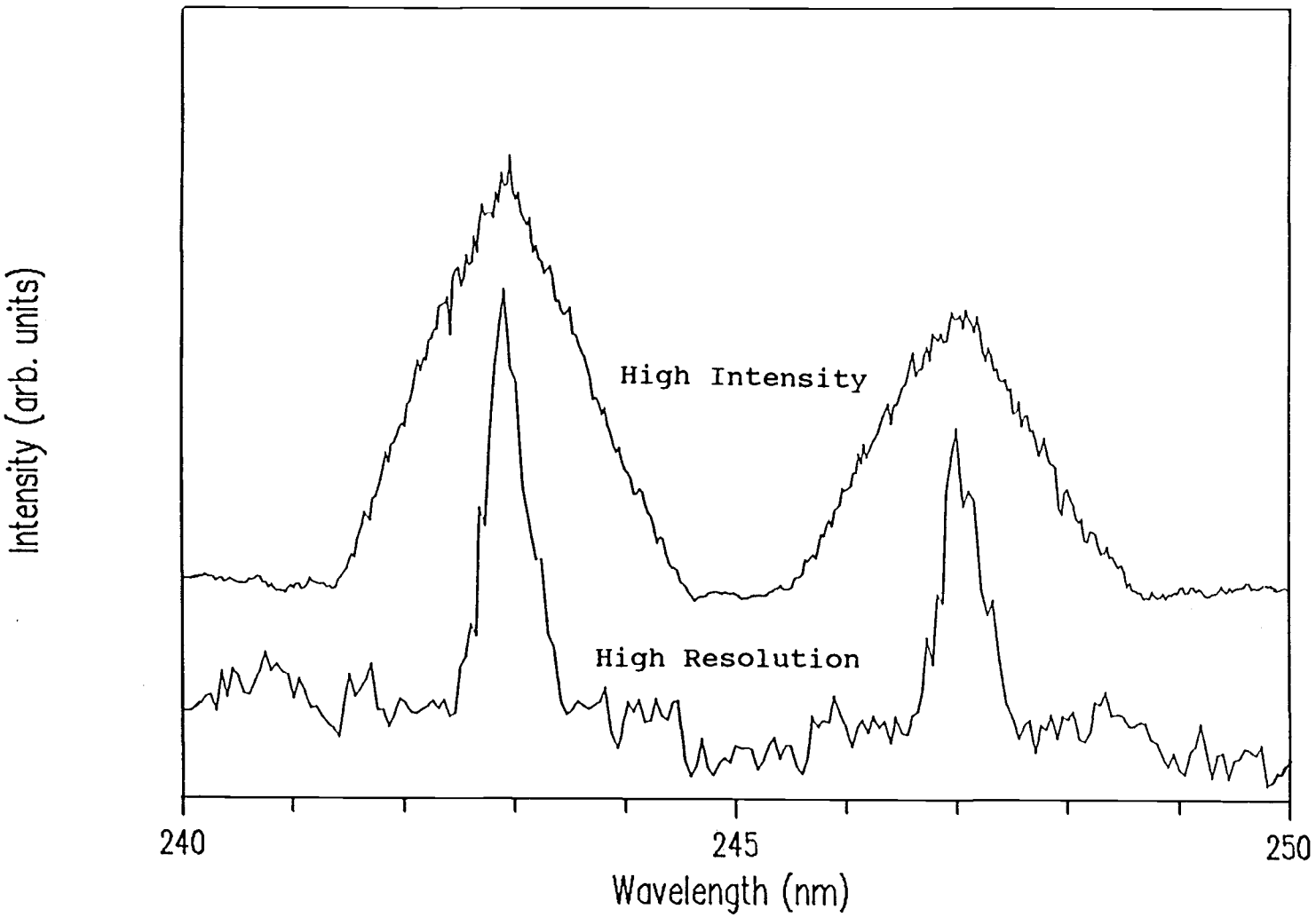

Fig. 15 Spectrum of second order krypton and Lyman-α lines.

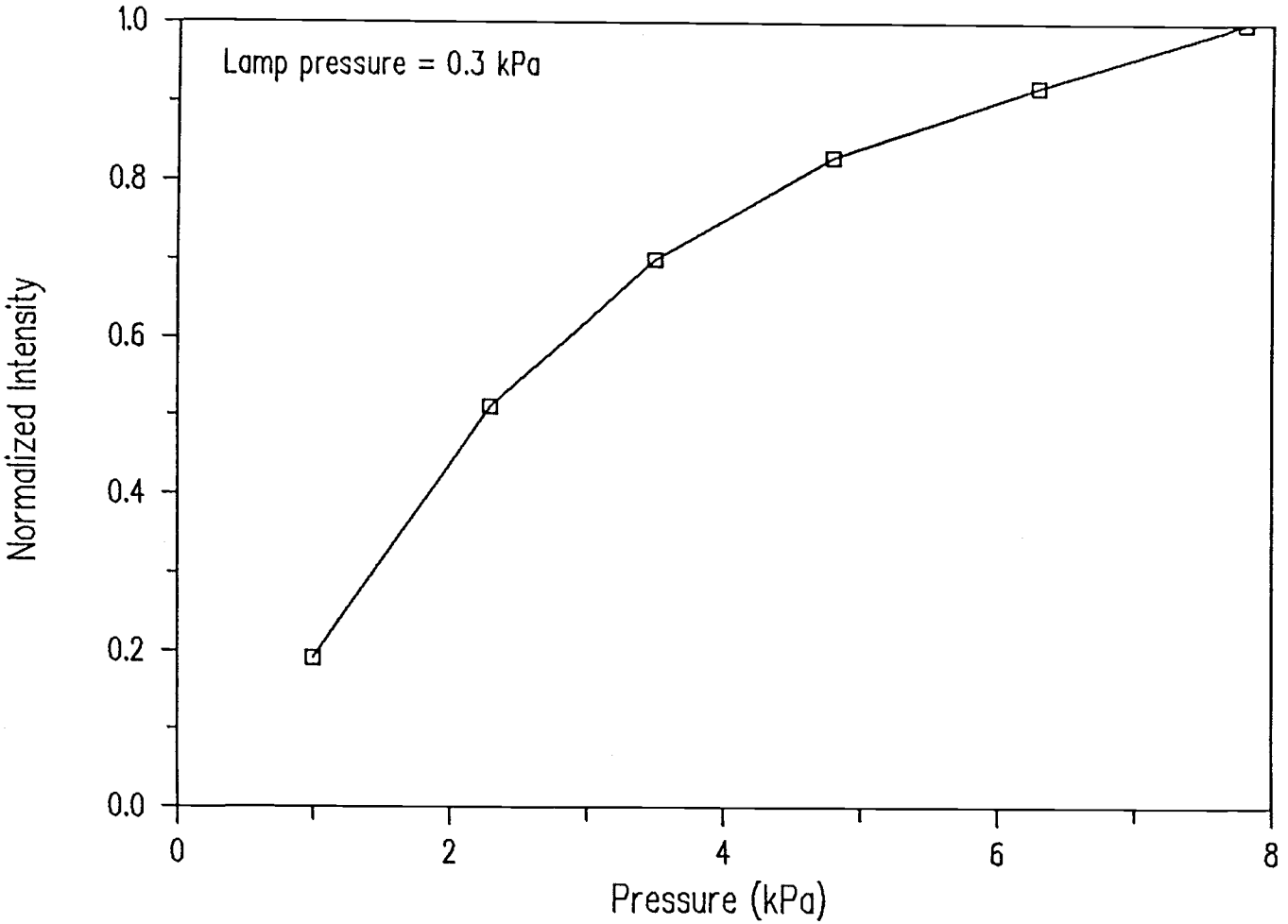

Fig. 16 Variations of Lyman-α signal strength with emitter gas supply pressure.

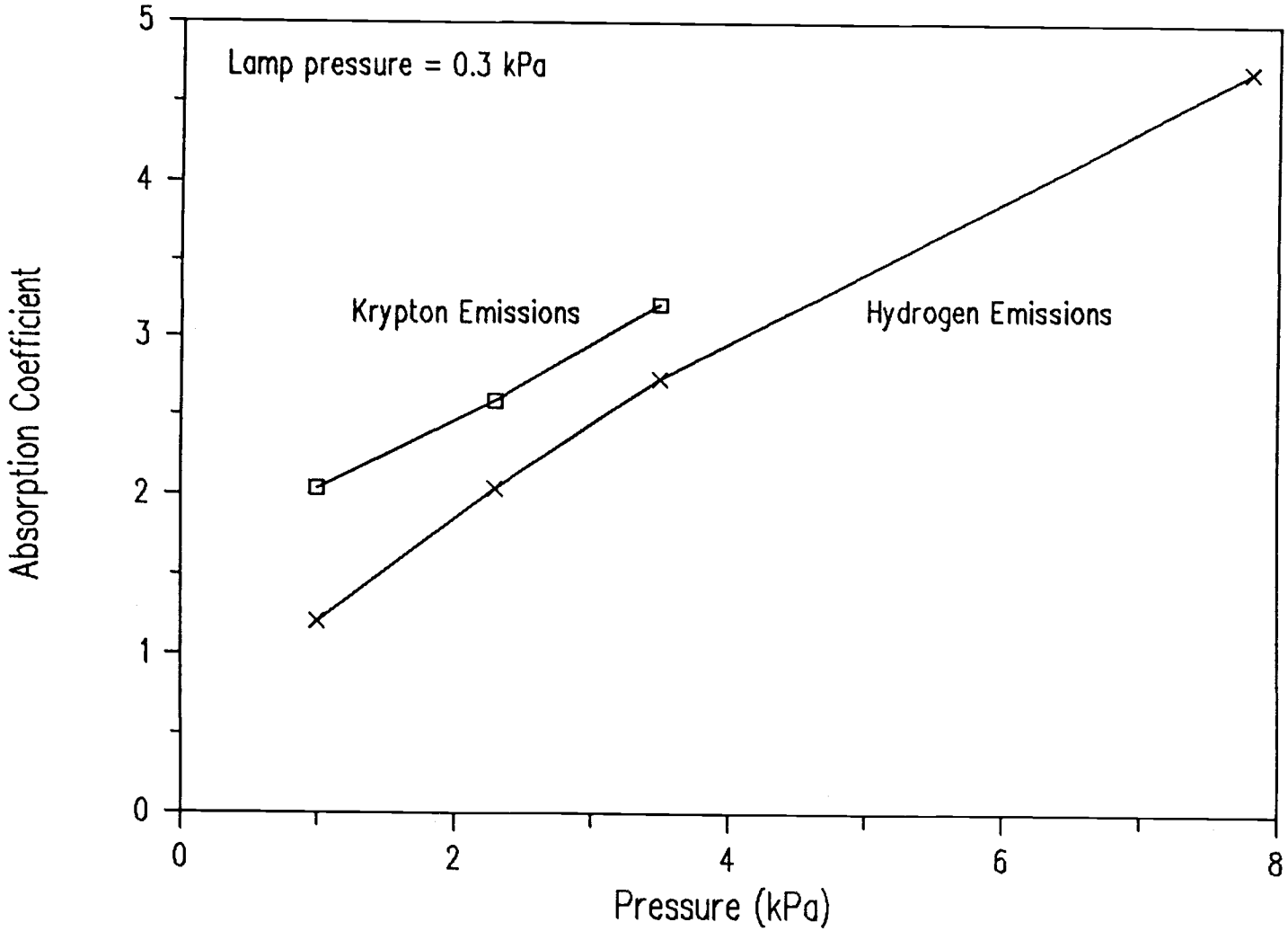

Fig. 17 Variations of K_{OL} with emitter gas supply pressure.

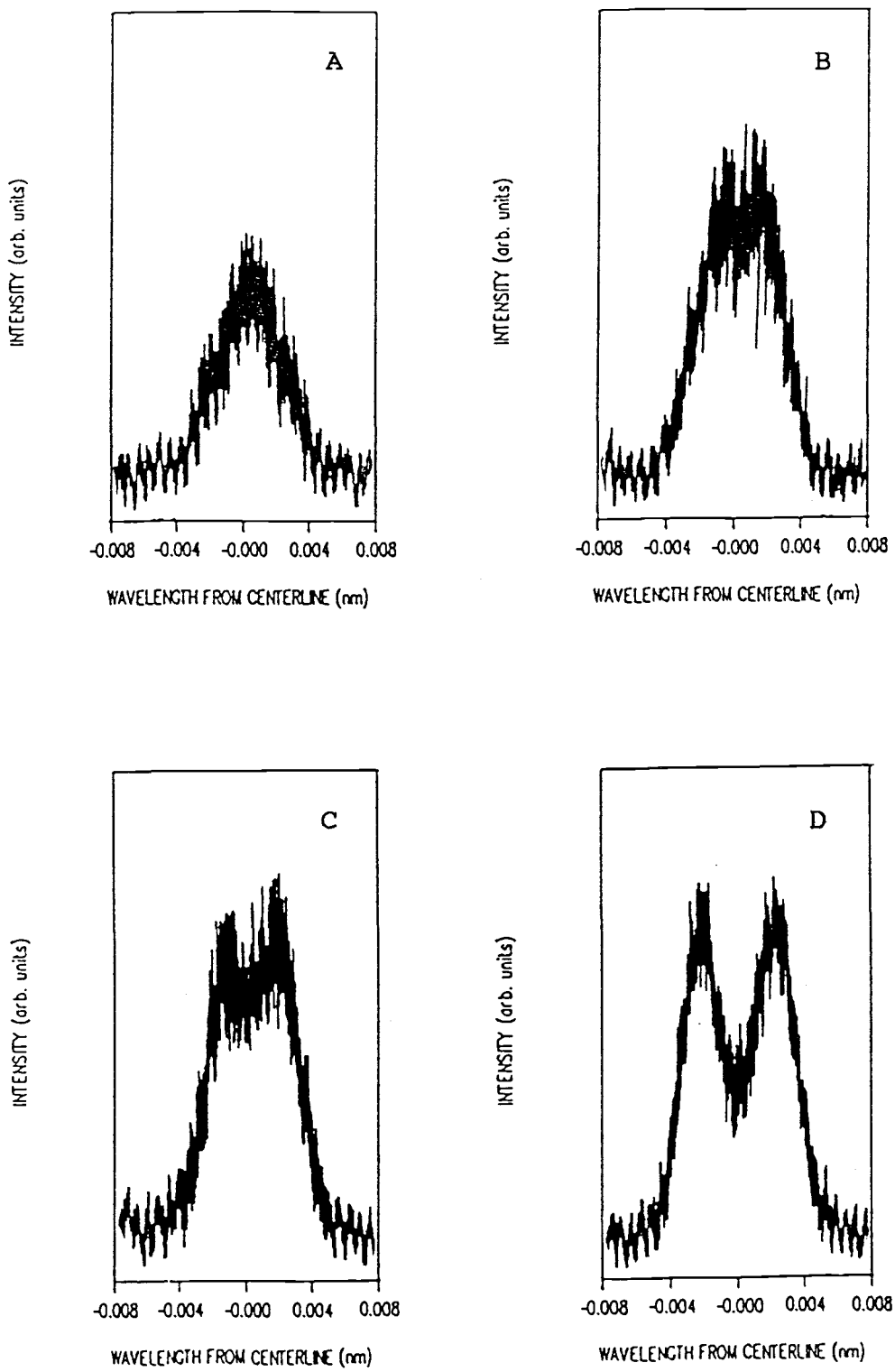

Fig. 18 Spectra recorded from high resolution scans of the 47th order hydrogen Lyman-α line.

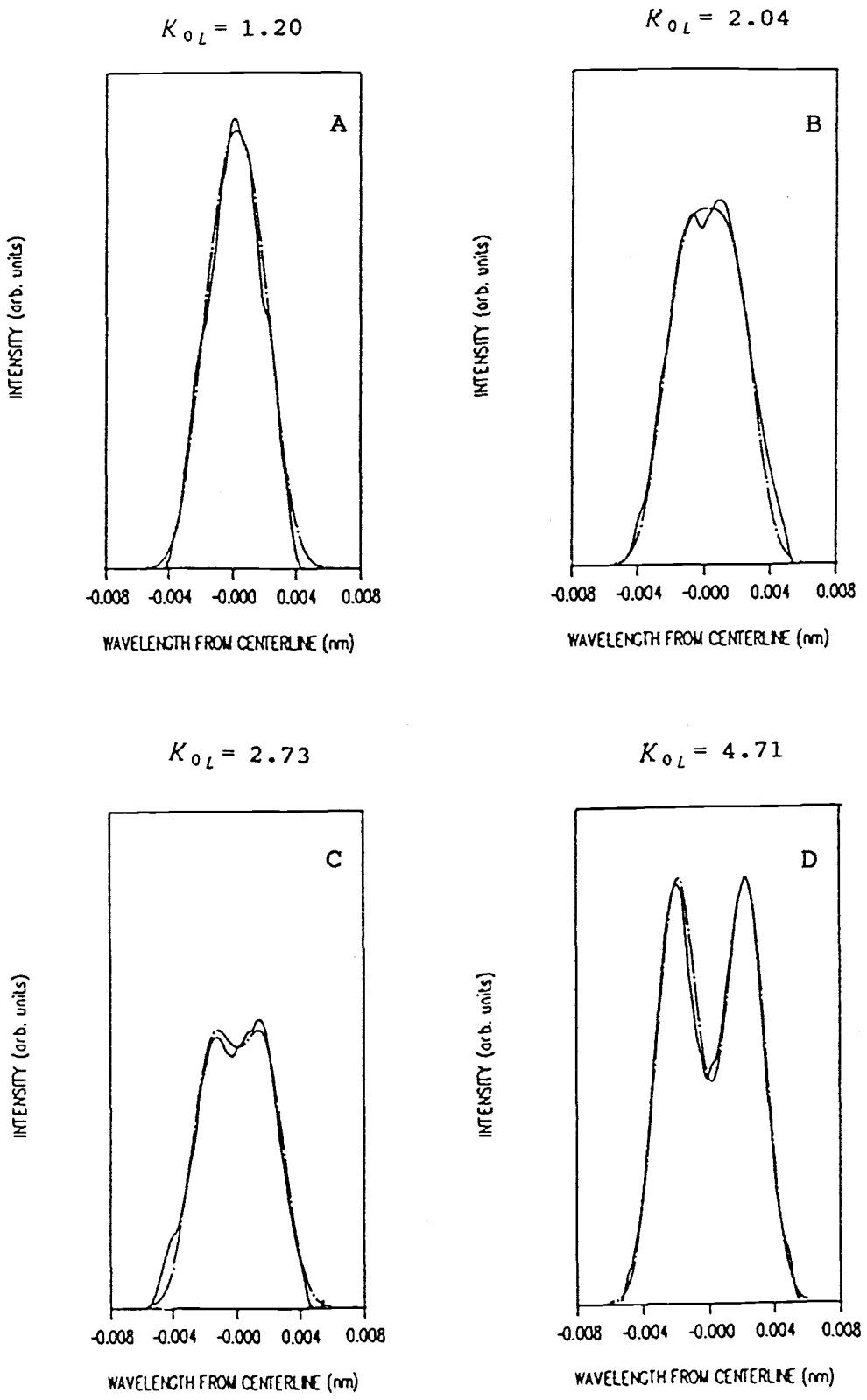

Fig. 19 Digitally smoothed hydrogen spectra along with model predictions.

numerically smoothed profiles obtained from these spectra are shown by the solid curves in Fig. 19. Signal intensities were recorded digitally at a rate of 10 Hz during 0.1 nm/min scans (this corresponds to 282,000 samples/nm after correcting for operation in the 47th order). Relatively high noise levels exist in the unsmoothed spectra, in spite of signal conditioning with a 100 Hz low-pass filter. This weak signal was due to the extremely narrow monochromator slit-width selected (0.04 mm for both the inlet and outlet slits). The high frequency character of the noise, however, allowed digital filtering to produce the smooth curves shown in Fig. 19. In these curves, it can be seen that plots with high absorption coefficients exhibit the self-absorbed profile discussed earlier. As was expected, the degree of self-absorption was found to increase with lamp pressure.

For all spectra, the frequency scale was calibrated by recording a spectrum containing the 47th order hydrogen and deuterium lines. It is known that the separation between these peaks is 0.0329 nm (Lifshitz, 1977), which allowed the wavelength scale for all spectral measurements to be set. The spectrum of the 47th order Lyman-α hydrogen and deuterium lines is presented in Fig. 20.

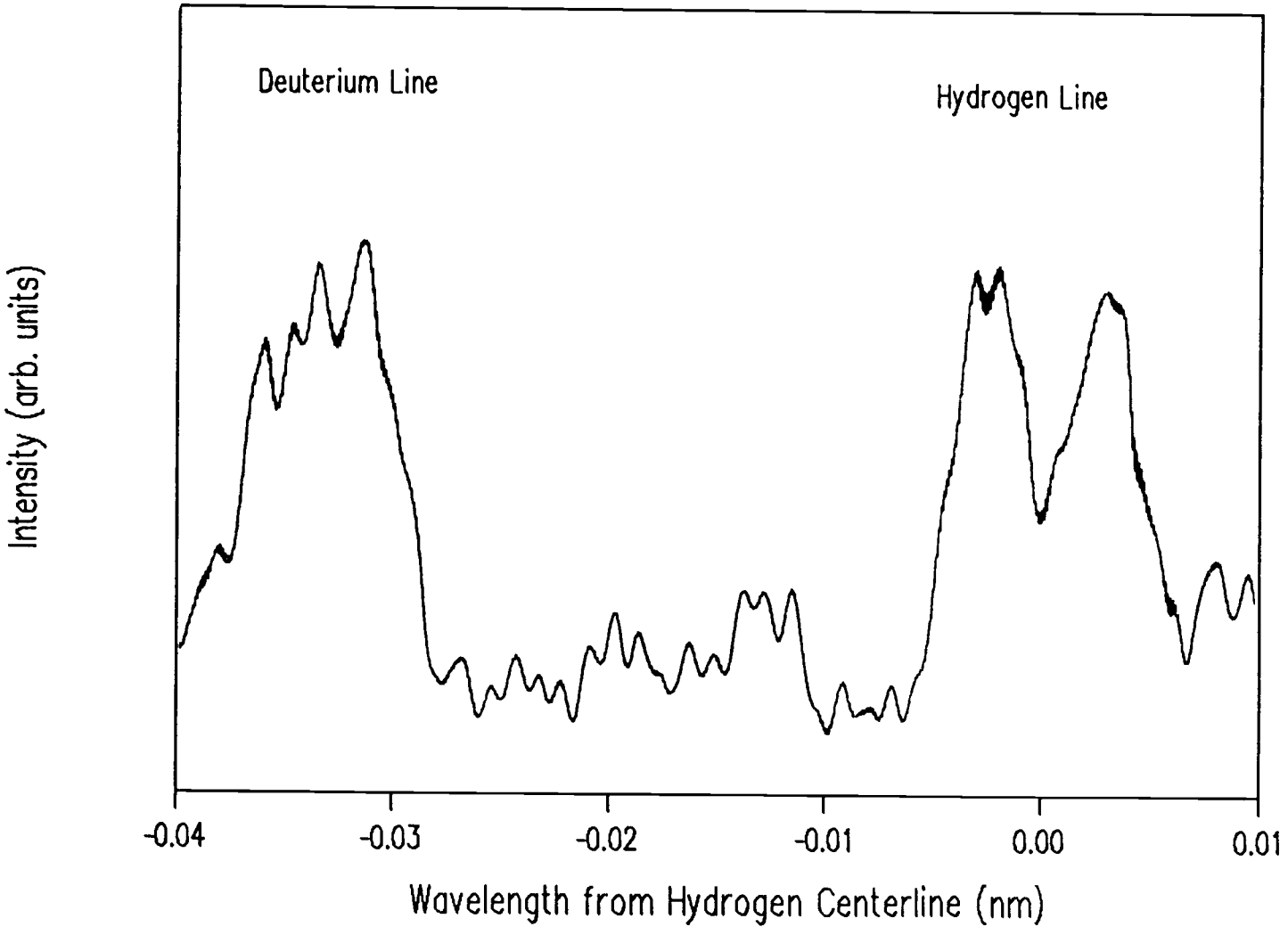

Fig. 20 Spectrum containing 47th order hydrogen and deuterium Lyman-α lines.

As discussed earlier, the profiles presented in Fig. 19 are not accurate representations of the actual lines emitted from the lamp. Line broadening and reduction in definition occur due to the instrument function of the monochromator. As with any spectral device, the monochromator does not resolve radiation at specific frequencies, but instead passes radiation in a narrow bandwidth. During a scan of a resonant line, the monochromator grating is rotated so that this band moves steadily across the emitting frequencies. If the emission line is much broader than the bandpass of the instrument, little distortion of the spectrum occurs. However, if the line is narrower than the bandpass, the resulting line bears little resemblance to the actual profile.

In this study, an estimate of the bandpass of the instrument was made using the measured linewidth of the 116.5-nm krypton resonance line. The procedure was as follows:

* A prediction of the expected width of this line was made by scanning the 47th order of the Lyman-α line, then correcting for krypton's reduced Doppler broadening.
* This calculated width was then compared to the recorded linewidth.

The linewidth recorded for krypton, however, was 0.003 nm while the predicted width was .0008 nm. This meant the width of the measured profile was primarily due to broadening caused by the instrument function of the monochromator, thus allowing the measured lineshape to be used as a calibration of the instrument function. The relative widths of the instrument function and a typical hydrogen emission spectrum, are illustrated by the spectra presented in Fig. 21.

Values of T_L were then obtained from fits of the model profiles to the recorded spectra. For reasons of numerical stability and simplicity, computational lineshapes were convoluted with the instrument function and fit to measured spectra, instead of deconvoluting the experimentally recorded lineshapes and performing fits. Model profiles after convolution, using the best fits of T_L and K_{0L} (for hydrogen), are shown as the dashed lines in Fig. 19.

An analysis of the spectra showed the best fit for all spectra occurred for a T_L of 1100 K. The constant value is explained by noting that T_L is primarily dependent on the lamp power and gas pressure, both of which were kept constant, while the relative flow rates of the two lamp gas supplies were varied. In these fits, it was observed that the most reliable indication of

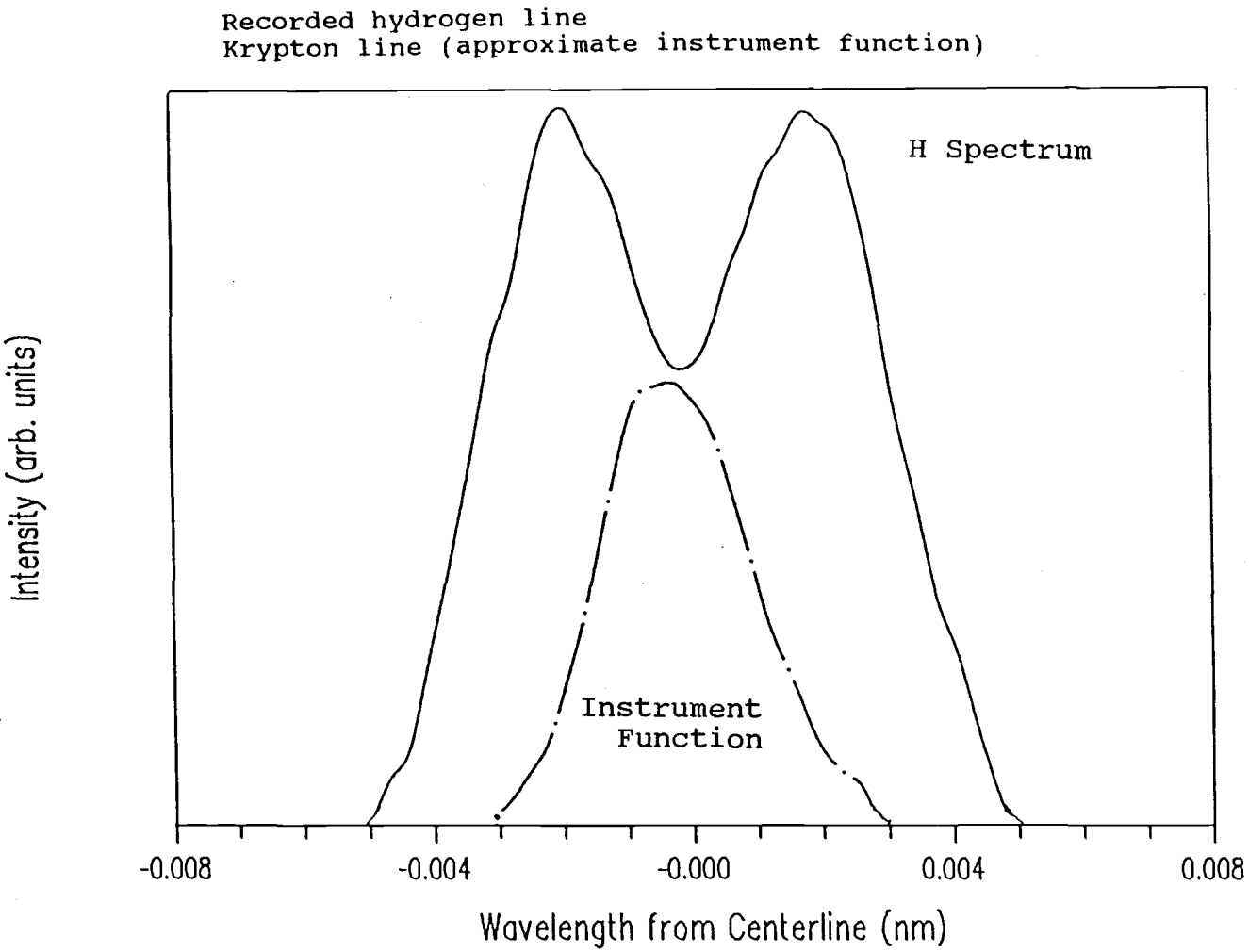

Fig. 21 Recorded hydrogen emission line along with the monochromator instrument function

lamp temperature was found in the highly self-absorbed profiles. For these spectra, the frequency separation between the two maxima is very weakly dependent on K_{0L}, and is primarily a function of T_L. This measure was also found to be insensitive to small errors in the evaluation of the instrument function.

For the krypton lamp emission profile, the second model parameter, K_{0L}, was evaluated by resonant absorption measurements and will be discussed in the following section.

4.4.3 MODEL VALIDATION

The accuracy of the proposed model in evaluating temperatures was confirmed by a series of steady state absorption measurements. The steady state apparatus described earlier was used to deliver a gas composed of 1% Kr in N_2. Resonant absorption at the Kr emission line of 123.5 nm, along with the pressure of the absorbing sample, were recorded for eight gas temperatures between 305 K and 580 K. Temperatures above ambient were generated by resistively heating the gas delivery tube.

An independent measurement of the temperature of the absorbing gas was made by a two step process. In the first step, temperatures in the gas delivery tube during resonant absorption measurements were recorded by means

of a chromel-alumel thermocouple positioned inside the tube. Temperatures of the sampled gas were then determined in a separate set of experiments. This was accomplished by placing a second chromel-alumel thermocouple inside the vacuum chamber within 1 mm of the orifice. The values measured by this thermocouple were recorded over the same range of gas supply tube temperatures and flow rates used in the absorption experiments. This allowed the two temperature measurements to be correlated as shown in Fig. 22. For both sets of measurements, the supply gas flow rate was maintained by controlling the pressure in the gas delivery tube, while in the second set, the pressure of the gas surrounding the second thermocouple was raised to 2 kPa (12 Torr) in order to achieve accurate temperature readings. This pressure was achieved by extending the flow tube to touch the combustion chamber endplate, constricting the flow tube exit orifice to less than a 1 mm diameter, and evacuating the vacuum chamber with the mechanical vacuum pump.

Table 4 shows a comparison of the sample temperatures obtained from this correlation, with the temperatures predicted from krypton absorption measurements. The predictions were made using a value of 0.16 for the oscillator strength (Zaidel, 1970), a lamp

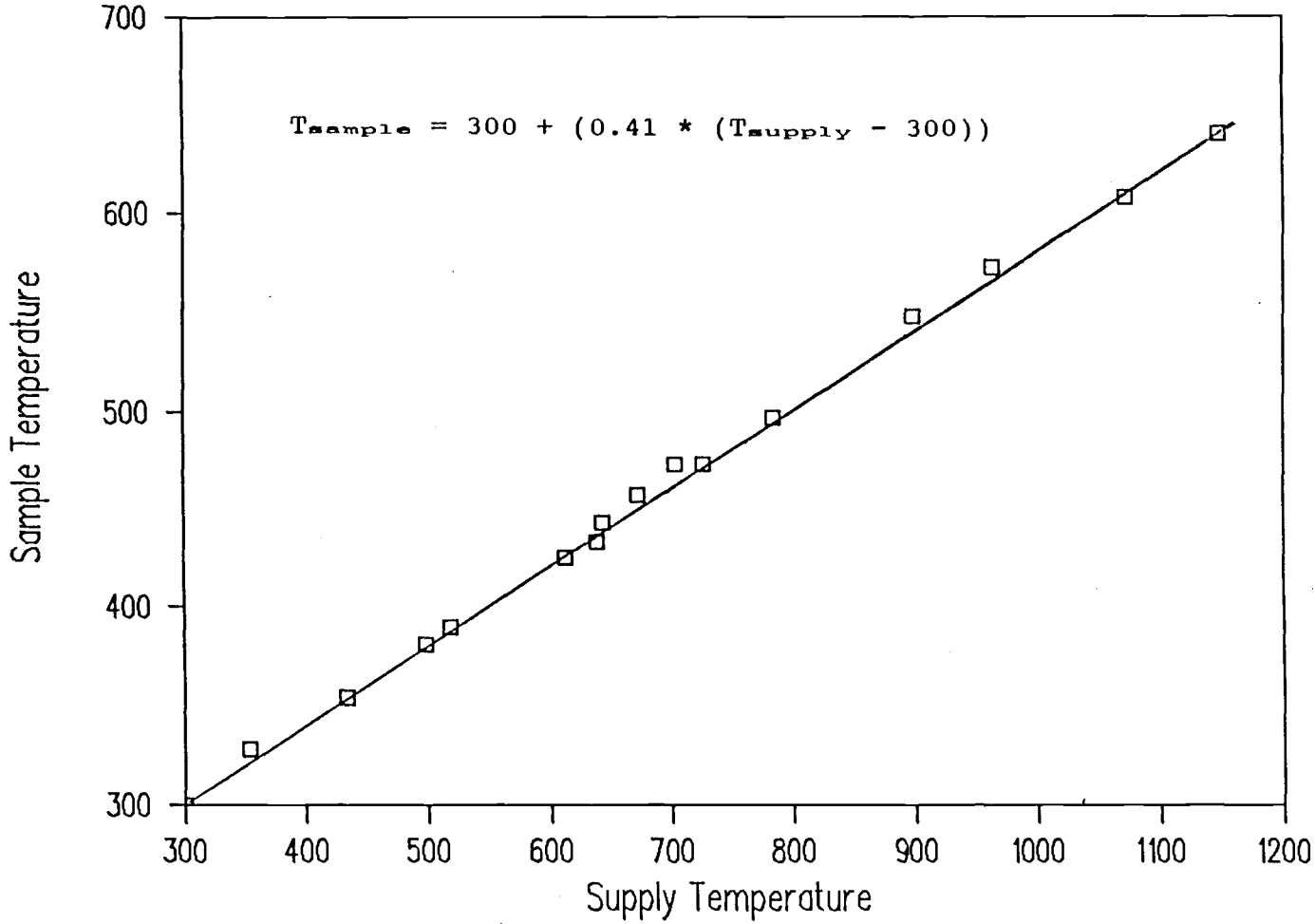

Fig. 22 Correlation of measured temperatures used in validating model.

Table 4

Recorded and Predicted Temperatures
for the Steady State Experiment

Recorded Temperature	Predicted Temperature	Absorption Fraction	Flow Tube Pressure
305 K	305 K	0.417	25.7 Pa
338 K	348 K	0.456	26.6 Pa
384 K	382 K	0.472	24.7 Pa
414 K	409 K	0.485	23.9 Pa
451 K	432 K	0.495	23.3 Pa
523 K	514 K	0.533	22.5 Pa
550 K	554 K	0.548	22.3 Pa
578 K	565 K	0.550	22.0 Pa

temperature of 1100 K, and a K_{0L} of 4.2. This latter value was obtained by matching the predicted and measured absorption at 305 K. These values, along with the measured absorption levels and the flow tube pressures, were then used in the model to generate a corresponding temperature at each of the seven elevated thermocouple readings.

The absorption fraction shown in Table 4 was observed to increase with increasing temperature. This runs contrary to the decrease in absorbing atom density caused by the temperature rise. An absorption increase can be explained by noting that, due to the high emission temperature, the lamp profile is much broader than the sample absorption linewidth. As a consequence, effective absorption only occurs at the center of the emission band, leaving the wings relatively unaffected. Increasing absorption with temperature is therefore observed because, as the sample temperature increases, the width of the absorption line expands and a larger portion of the emission line is subject to absorption.

Another trend observed in the experiments was a decrease in flow tube pressure with increasing temperature. Such a decrease is expected, since gas dynamic theory predicts a $1/\sqrt{T}$ dependence of the mass flow rate through a sonic orifice. An exception to this

pattern is found in the first pressure value. To avoid overloading the diffusion pump at this temperature, the flow rate through the gas delivery tube was reduced. This resulted in a slightly lower stagnation pressure at the sampling orifice, and a corresponding low pressure reading in the delivery tube. Higher flow rates were used with heated gases to minimize heat transfer and boundary layer effects at the orifice.

Table 4 demonstrates that predicted and recorded temperatures remain relatively close throughout the temperature range. Deviations do not appear to be systematic and can be attributed to uncertainty in the measurement of absorption values. The necessity of passing radiation through three Mg-F windows caused attenuation to the point where noise from the PMT was significant. Even after time averaging, variations as large as 1% were seen between consecutive data sets (absorption values presented in Table 4 are the result of averaging three sets of 2500 data points, each collected at a sampling rate of 2000 Hz). Variations are important because small deviations in absorption lead to significant changes in the predicted temperature. For example, the model temperature of 432 K rises to 450 K when an absorption fraction of 0.503 is used in place of the recorded value of 0.495.

4.4.4 TRANSIENT COMBUSTION TEMPERATURES

The capability of this new diagnostic technique to track rapid changes in temperature was demonstrated by experiments in which a propagating flame was studied. To produce such a flame, the combustion chamber was filled to a pressure of 25 kPa (190 Torr) with a stoichiometric hydrogen/air mixture. Ignition was initiated at the nichrome coil producing a flame which propagated throughout the combustion chamber. A plot of the pressure in the chamber during combustion is shown in Fig. 23. Absorption in the flow tube during many repetitions of the combustion event was measured using three different lamp profiles for both orifice configurations. When the foil sampling orifice was used, the combustible mixture contained a 0.20% mole fraction of krypton, while for experiments employing the conical orifice, the mixture contained a 0.40% mole fraction of krypton. Plots of absorption and flow tube pressure during combustion are presented in Figs. 24 and 25 for the foil and cone orifices respectively. Each absorption curve is the result of signal averaging 10 experimental runs and the pressure traces are averages of 5 runs.

The combustion event occurring near the sampling orifice can be divided into periods before and after the arrival of the flame front. Before the front's arrival,

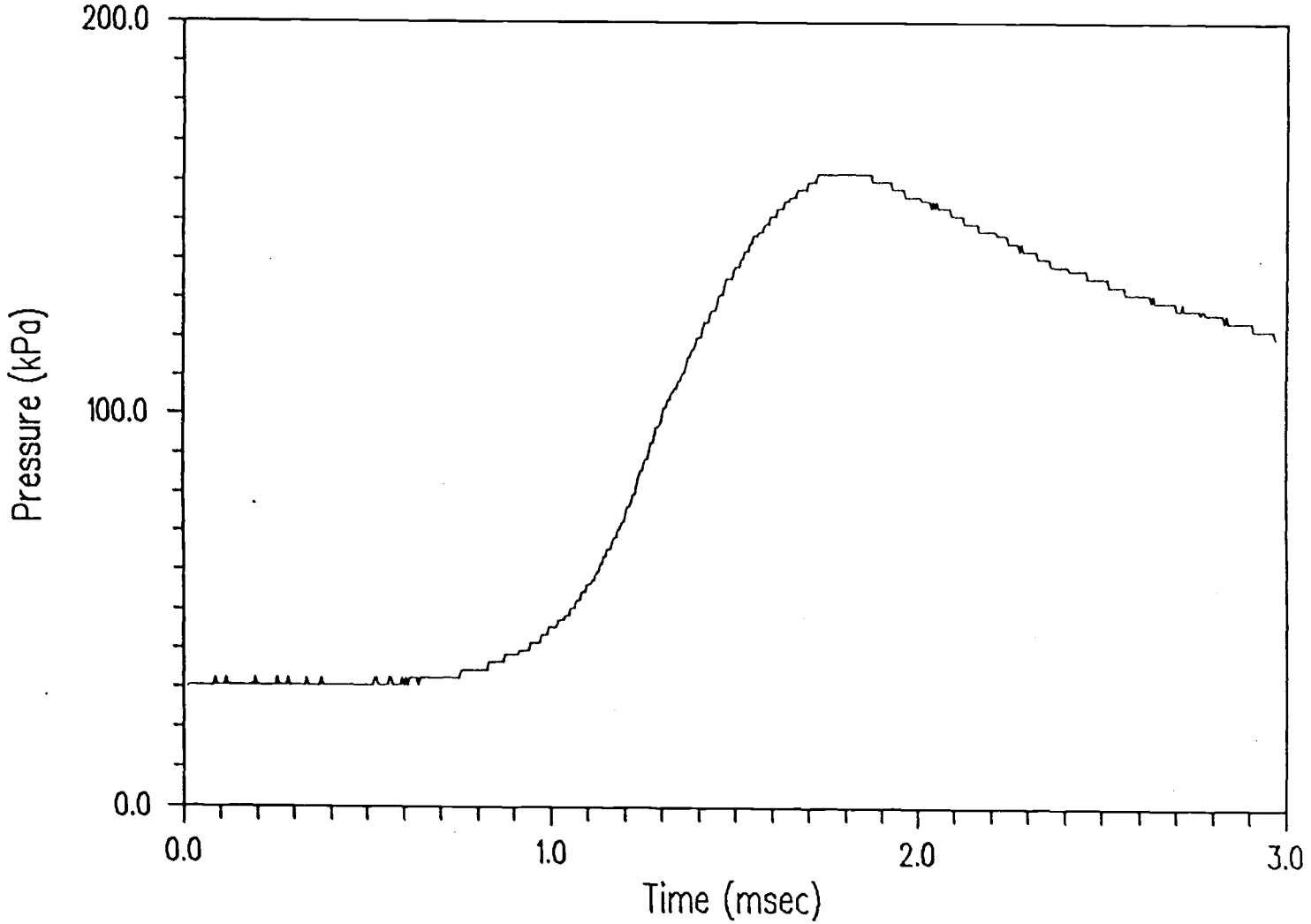

Fig. 23 Chamber pressure during DSARAS experiments.

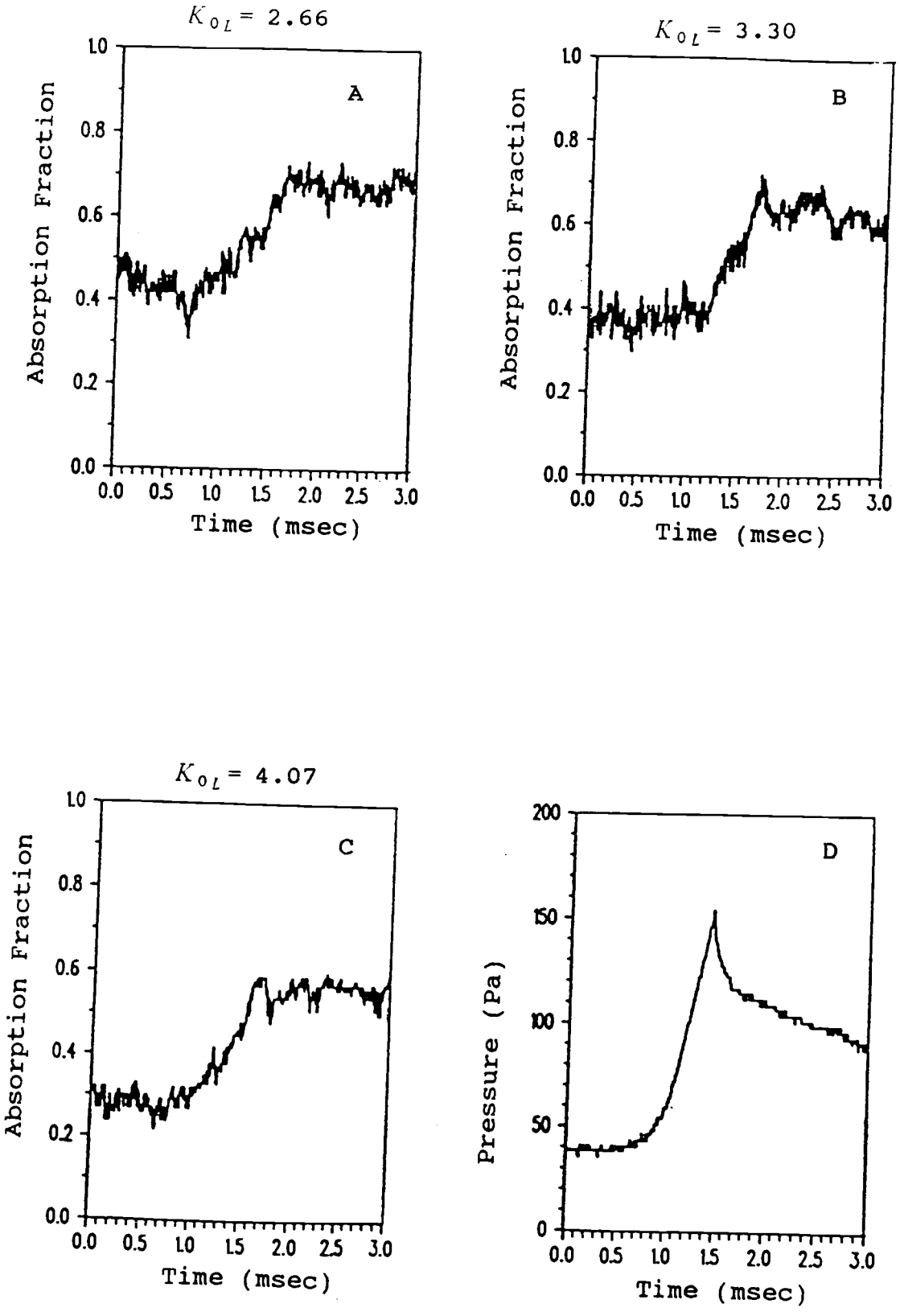

Fig. 24 Resonant absorption by krypton and flow tube pressure for foil sampling orifice experiments.

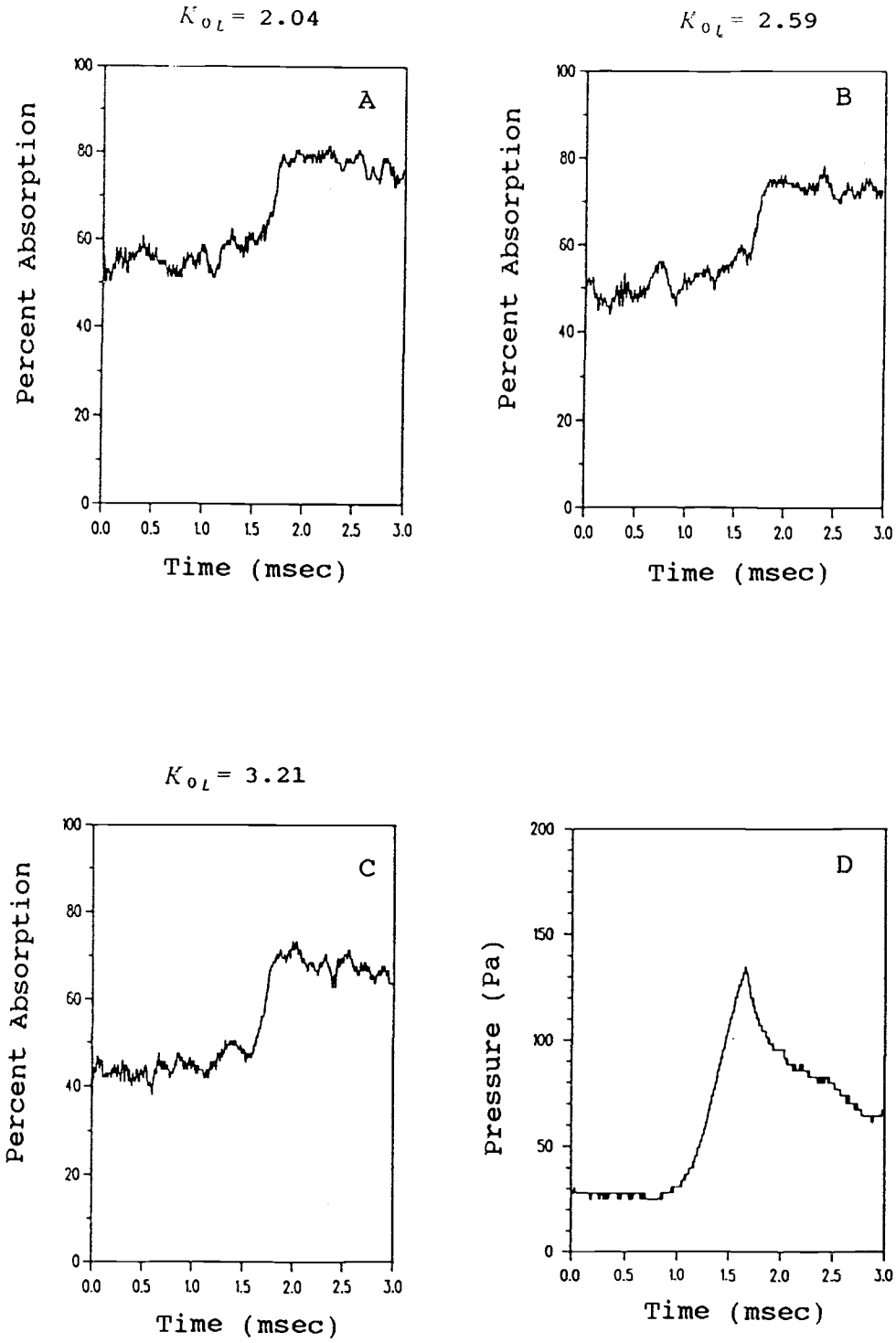

Fig. 25 Resonant absorption by krypton and flow tube pressure for conical sampling orifice experiments.

the chamber pressure increased due to the compression caused by the flame propagation, however during this period the sampled gas was comprised of cool, unburned reactants. The flame front's arrival at the orifice was responsible for an extremely abrupt rise in temperature, after which hot product gases were sampled. This localized temperature increase had little effect on the overall chamber pressure, implying an abrupt drop in density accompanied the flame passage.

The flow tube pressure curves in Figs. 24 and 25 show the effects of flame propagation. During the early stages of combustion, the rise in pressure was similar to that in the chamber. However, an abrupt decrease occurred at 1.5 msec and 1.7 msec for the cases of the brass and cone orifice arrangements respectively. This drop coincided with the arrival of the flame front, and it was caused by the decrease in mass flow through the orifice induced by the rapid increase in the sample temperature. The gradual decrease in pressure after the flame's arrival was due to cooling of the product gases inside the chamber. Differences in flame arrival time recorded with the two orifice configurations can be attributed to the variation in chamber geometry accompanying the change of orifice plates. This change also caused the chamber pressure at the time of the

flame's arrival to differ. It was 105 kPa (790 Torr) for the foil orifice runs and 130 kPa (980 Torr) for the conical orifice runs.

For each orifice configuration, absorption measurements were recorded using three lamp emission profiles in order to obtain independent estimates of temperature during combustion. Agreement between the predicted temperature time-histories was used to provide further confirmation of the validity of the technique. In this analysis, T_L was set to 1100 K. In obtaining K_{0L}, it was assumed that before ignition the sample had a temperature of 300 K and that the initial absorption and flow tube pressure could be approximated by their averages over the first 0.5 msec of the recorded event. Employing the derived lamp parameters, temperatures at 0.1-msec intervals throughout combustion were calculated. It should be noted that, due to the chemical reaction, the Kr mole fraction of the product gases was taken to be 15% higher than that for the reactants. Figure 26 displays the time resolved averages of the predicted temperatures for both orifice arrangements. The standard deviation of the predictions was approximately 20 K before the arrival of the flame front, and approximately 75 K after the arrival. The jump in the standard deviation accompanying the arrival

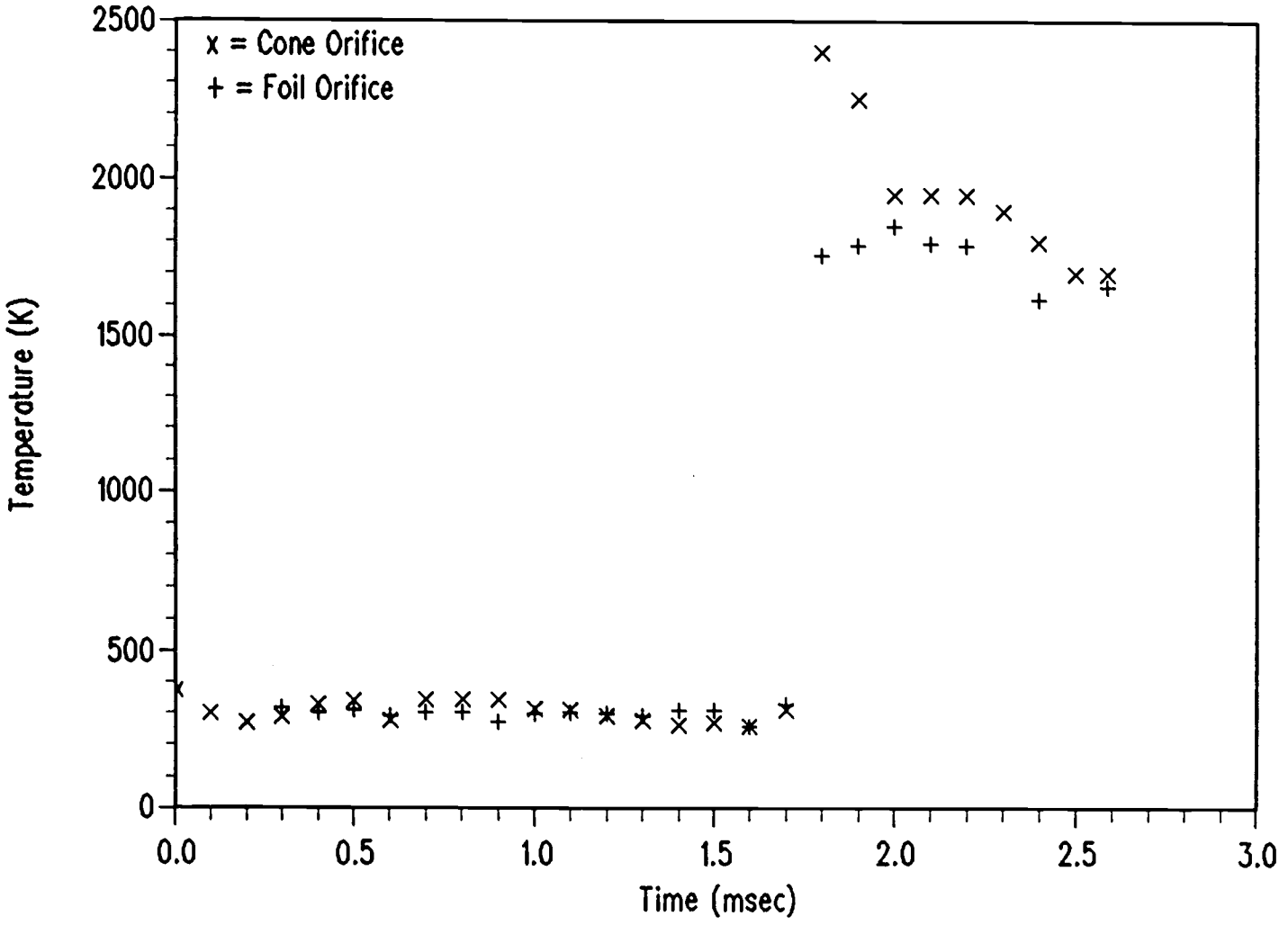

Fig. 26 Predicted temperatures during combustion.

of the flame front was not caused by greater noise levels in the absorption signal, but instead was caused by a greater sensitivity in the model to absorption changes at high temperatures. For both source arrangements, the deviation between predictions is relatively small, considering the noise levels associated with the absorption measurements.

Temperatures in Fig. 26 remain at 300 K until the arrival of the flame front. It should be noted that in this figure the time axis for the foil orifice experiments was shifted so that the arrival of the flame front was coincident for both cases. Differences in maximum temperatures obtained with the two orifices can be explained by noting that the quenching distance for the flame was greater than the orifice diameter. Quenching has been shown to be of minor importance when conical orifices are employed (Biordi, 1977, Yoon and Knuth, 1979; Hayhurst et al., 1977), however when the brass foil orifice was used, the flame was extinguished before reaching the endwall. This resulted in a lower apparent flame temperature due to mixing of the flame gases with those from the unburned boundary layer. In the case of the conical orifice, the maximum temperature is very close to that which is calculated for an adiabatic flame.

Temperature values during the passage of the flame front (between 1.7 and 1.8 msec) are not presented. Reliable absorption values in this region were not obtained due to the high noise level and uncertainties in signal averaging. For individual runs, it was very difficult to determine the exact time of the flame's arrival, and errors of up to 50 μs were possible. This lead to a loss of resolution of the averaged absorption signal.

4.4.5 ATOMIC HYDROGEN MEASUREMENTS

The capability of this new diagnostic technique to track the rapid evolution and decay of free radicals produced by the passage of the flame front was also studied. Absorption of Lyman-α radiation in the flow tube during many repetitions of the combustion event was measured using three different lamp profiles. These experiments were conducted using both the brass foil and quartz cone sampling arrangements. Plots of absorption and flow tube pressure during combustion obtained with the foil sampling orifice are presented in Fig. 27, and Fig. 28 displays the values recorded using the conical orifice. Each absorption curve is the result of signal averaging 10 experimental runs, and the pressure traces are averages of 5 runs.

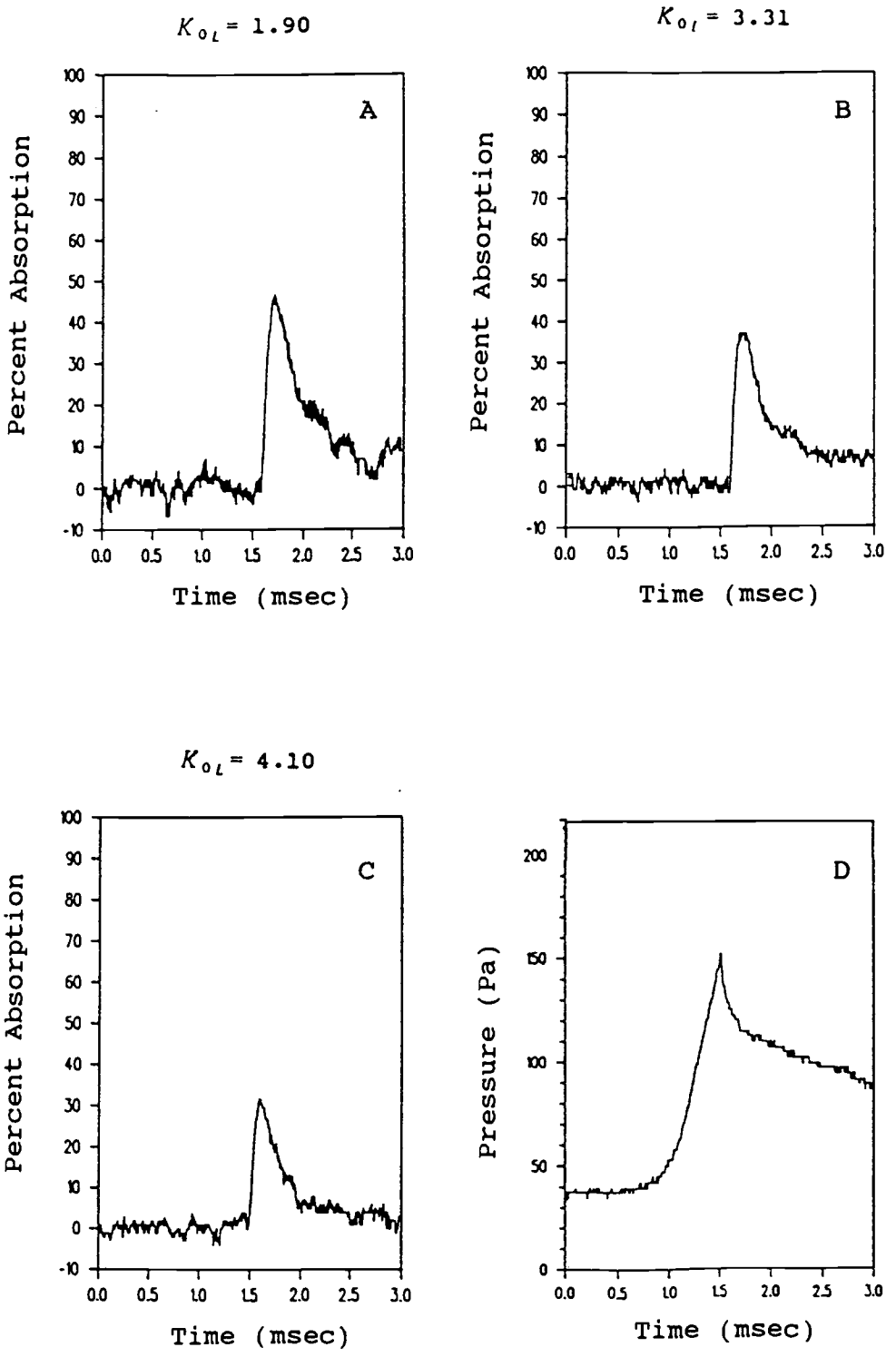

Fig. 27 Resonant absorption by atomic hydrogen and flow tube pressure for foil sampling orifice experiments.

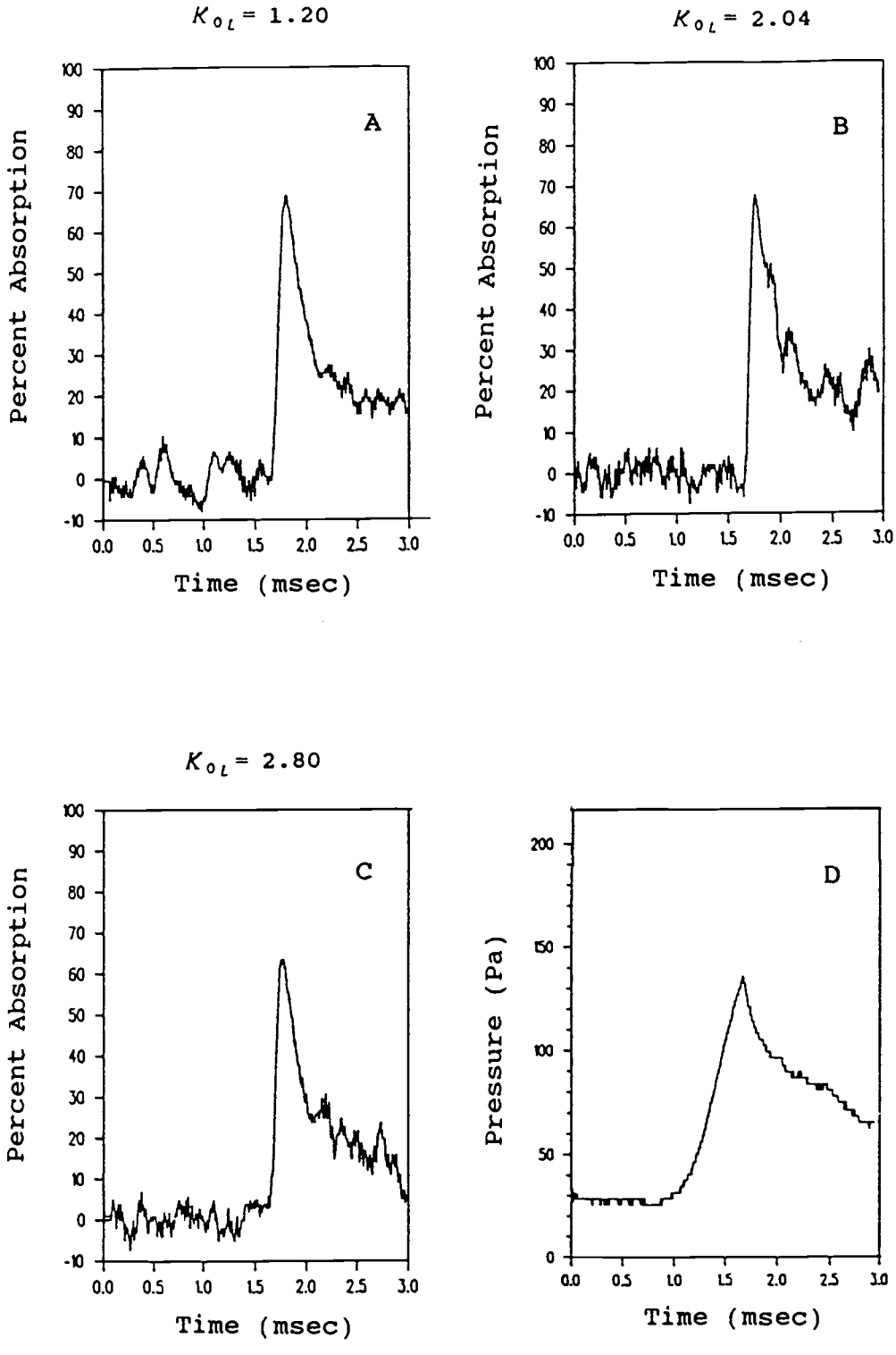

Fig. 28 Resonant absorption by atomic hydrogen and flow tube pressure for conical sampling orifice experiments.

These pressure and absorption signals, along with the numerical lamp profiles and calculated temperatures, were then used to obtain hydrogen atom mole fractions. Figure 29 displays the mole fractions predicted for both orifice configurations using each of the three lamp profiles. As expected, a higher atomic hydrogen fraction was obtained using the quartz orifice. For the case of the foil orifice, low values were the result of several factors including; dilution of the flame gases with unburned reactants from the boundary layer, and disappearance of atomic hydrogen through gas phase and wall-induced reactions. Concentration values during the arrival of the flame front are not presented due to the uncertainties in calculating temperatures in this interval.

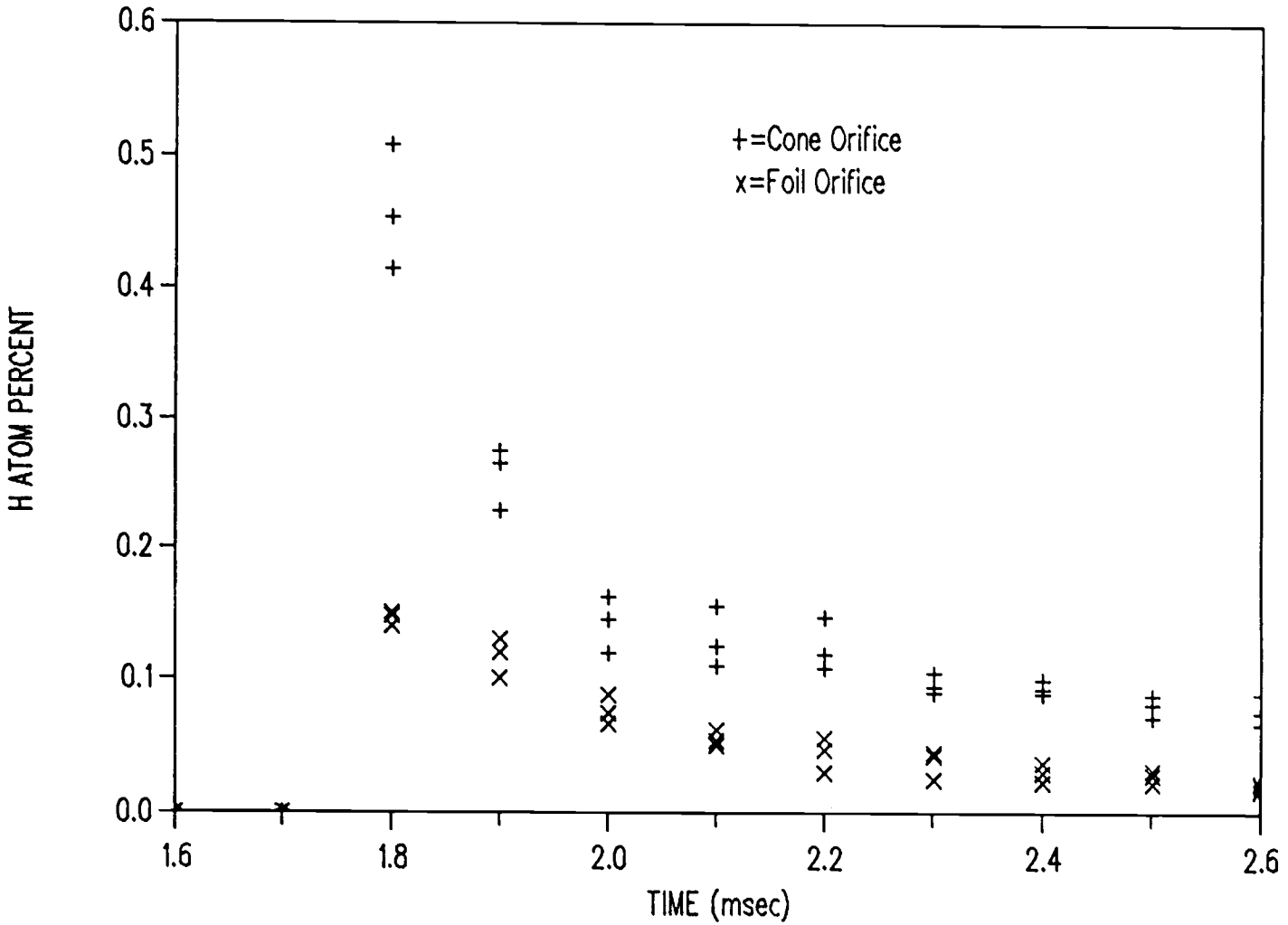

Fig. 29 Hydrogen mole fractions during combustion.

Chapter 5: CONCLUSIONS

This study has demonstrated that the direct sampling optical analysis technique provides for species and temperature detection with a previously unachievable degree of time resolution. Of the two spectroscopic analysis techniques, atomic absorption holds more promise since the ability to measure both temperatures and atomic species concentrations in transient events could lead to significant advances in engine design and the formulation of fuels.

Although obtaining temperatures and atomic radical concentrations by the atomic absorption technique appears complex, it relies on just two major assumptions. In this study, efforts were made to check the validity of both. The first assumption was that the emissions from the lamp could be modeled as an emitting region followed by an absorbing region, thus allowing the emission profile to be characterized by two parameters. The validity of this model was demonstrated by the close fit between predicted and recorded hydrogen spectra.

The second assumption was that the absorption by a sample in the flow tube could be characterized as having

a thermal doppler profile at a temperature equal to that of the sampled gas. This assumption was verified by a series of steady-state temperature measurements.

The focus of this study has been to demonstrate the feasibility of the DSARAS technique as a tool for investigating transient combustion processes. The promise of the technique has been demonstrated, however significant opportunities exist for improvements in its implementation. At this stage in its development, the technique is time consuming due to the necessity of obtaining and analyzing Lyman-α lamp emission profiles. Further work needs to be conducted in characterizing and standardizing the performance of resonance lamps. Ideally, a lamp with known emission characteristics could be manufactured so that concentrations and temperatures could be derived from simple absorption measurements. In addition, an improved lamp design might allow wavelength selection to be performed by the use of frequency filters instead of vacuum monochromators. This would greatly decrease the cost of the apparatus, as well as increase the radiation intensity sensed by the PMT.

In any case, a major objective of further investigations should be to increase the signal-to-noise ratio of absorption measurements. To obtain temperature

and species concentration values during the actual flame passage, single run absorption time-histories must be achievable. One modification which could lead to improved signal strength is the replacement of the grating used in absorption experiments with one blazed for maximum efficiency around 120 nm. This would allow the intense first-order lines to be used in absorption measurements. In addition, moving the monochromator closer to the lamp would increase the signal intensity due to the $1/R^2$ dependence of signal intensity (where R is distance). Employing these modifications, an increase in signal strength of an order of magnitude should be attainable.

Another feature of the apparatus that needs refinement is the window design. One problem with the current design is the window between the lamp and the vacuum chamber loses its ability to transmit UV radiation after several hours of operation. To avoid this, the window could be replaced with a multi-capillary array. These arrays are comprised of a large number of very narrow glass tubes, which allow light transmission through the open tube centers. Even though these arrays contain a high fraction of void space, their small tube diameters provide for extremely low flow rates through the array. In the proposed

application, gas flow from the lamp to the vacuum chamber would be especially small due to the low lamp pressure.

Additional problems would be presented by the windows on the flow tube if a hydrocarbon combustion process were studied. Soot formation would tend to foul the windows after a small number of measurements. To overcome this, studies should be performed to determine if a geometry of the flow tube exists for which windows are not necessary. The use of capillary arrays on the flow tube is not advised due to the difficulty in maintaining their alignment, and to their susceptibility to soot fouling.

BIBLIOGRAPHY

Ashkenas, H., and Sherman, F. S., 1966, "The Structure and Utilization of Supersonic Free Jets in Low Density Wind Tunnels", in "Proceedings of the Fourth International Symposium of Rarified Gas Dynamics", Academic Press, New York, p. 84.

Becker, K., Stumpf, B. and Shultz, G., 1980, "Cross-Beam Investigations of the OH Emission Spectrum after Dissociative Excitation of Water by Electron Impact", Chem. Phys. Lett., Vol. 73, p. 102.

Bier, K., and Hagena, O., 1963, "Influence of Shock Waves on the Generation of High-Intensity Molecular Beams From Nozzle Sources", Rarefied Gas Dynamics (J. Laurmann, Ed.), Vol 1, p. 478.

Biordi, J. C., 1977, "Investigating The Fundamental Chemistry of Flames with Molecular Beam Mass Spectrometry", in Progress in Aeronautics and Astronautics, AAIA, New York, Vol. 53, pp. 125-152.

Boiteux, H., 1965, Flame Spectroscopy, Part II, J. Wiley and Sons.

Braun, W., Bass, A. W., and Davis, D. D., 1970, "Experimental Test of a Two Layer Model Characterizing Emission Line Profiles", J. of Opt. Soc. Am., Vol. 60, pp. 166-170.

Braun, W., and Carrington, T., 1969, "Line Emission Sources For Concentration Measurements and Photochemistry", NBS-TN476, Nat. Bur. Std.

Coe, D., Robben, L., and Cattolica, R., 1980, "Rotational Temperatures in Nonequilibrium Free Jet Expansion of Nitrogen", Phys. Fluids, Vol. 17, pp 706-714.

Davis, D. and Braun, W., 1968, "Intense Vacuum Ultraviolet Atomic Line Sources", Applied Optics, Vol. 7, pp. 2071-2074.

Deckers, J., and Van Tiggelen, A., 1959, "Ion Identification in Flames", Symp. (Int.) Combust., 7th, pp. 254-255.

Dekoven, B. M., Levy, D. H., Zegarski, B. R., and Miller, T. A., 1981, "Rotational Excitation in the Electron Ionization of Supercooled N_2", J. Chem. Phys., Vol. 74, pp. 5659-5668.

Erdman, P. W., and Zipf, E. C., 1982, "Low-Voltage, High-Current Electron Gun", Rev. Sci. Inst., Vol. 53, pp. 225-227.

Fenn, J. B., and Deckers, 1963, J., "Molecular Beams from Nozzle Sources", Rarefied Gas Dynamics (J. Laurmann, Ed.), Vol. 1, p. 497.

Hammel, B. B., and Willis, D. R., 1966, "Kinetic Theory of Source Flow Expansion with Application to the Free Jet", Phys. Fluids, Vol. 9, p. 829.

Hayhurst, A. N., Kittleson, D. B. and Telford, N. R., 1977, "Mass Spectrometric Sampling of Ions from Atmospheric Pressure Flames - II: Aerodynamic Disturbance of a Flame by the Sampling System", Comb. Flame, Vol. 28, pp. 123-135.

Hernandez, S. P., Dagdigian, P. J., and Doering, J. P., 1982, "N_2 Rotational Energy Distribution in Cold, Supersonic Beams from Electron Excited Fluorescence Measurements of N_2^+", Chem. Phys. Lett., Vol. 91, pp. 409-412.

Kantrowitz, A., and Grey, J., 1951, "A High Intensity Source for the Molecular Beam", Review Sci. Instr., Vol. 22, p. 328.

Knuth, E. L., 1973, Engine Emissions: Pollutant Formation and Measurement (Springer and Peterson Eds.), Plenum Press, New York, pp. 319.

Lazzara, C. P., Biordi, J. C. and Papp, S. F., 1973, "Concentration Profiles for Radical Species in a Methane-Oxygen-argon Flame", Combust. Flame, Vol. 21, p. 371.

Lifshitz, A., Skinner, G. B., and Wood, D. R., 1979, "Resonance Absorption Measurements of Atom Concentrations in Reacting Gas Mixtures. I. Shapes of H and D Lyman-α Lines from Resonance Sources", J. Chem. Phys., Vol. 70, pp. 5607-5613.

Lucas, D., Peterson, R., Brown, N. J., and Oppenheim, A. K., 1984a, "Molecular Beam Mass Spectrometer Sampling Of Flash Ignited Combustion", Symp. (Int.) Combust., 20th, pp. 1205-1211.

Lucas, D., Peterson, R., Hurlbut, F. C., and Oppenheim, A. K., 1984b, "Effects of Transient Combustion Phenomena on Molecular Beam Sampling", J. Phys. Chem., Vol. 88, pp. 4548-4552.

Maki, R. G., Michael, J. V., and Sutherland, J. W., 1985, "Lyman-α Photometry; Curve of Growth Determination, Comparison to Theoretical Oscillator Strength, and Line Absorption Calculations at High Temperature", J. Phys. Chem., Vol 89, pp. 4815-4821.

Marrone, P. V., 1967, "Temperature and Density Measurements in Free Jets and Shock Waves", Phys. Fluids, Vol. 10, pp. 521-538.

Massey, H., and Burhop, E., 1969, Electronic and Ionic Impact Phenomena, Clarendon Press, London, Vol. I, p. 170.

Michael, J. V., and Weston, R. E., 1966, "Determination of Hydrogen Atom Concentrations By Lyman-α Photometry", J. Chem. Phys., Vol. 45, pp. 3632-3641.

Milne, T. A., and Green, F. T., 1966, "Mass Spectrometric Studies of Reactions in Flames. II. Quantitative Sampling of Free Radicals from One-Atmosphere Flames", J. Chem. Phys., Vol. 44, pp. 2444-2449.

Morse, F. A., and Kaufman, F., 1965, "Determination of Ground-State O, N, and H by Light Absorption and Measurement of Oscillator Strengths", J. Chem. Phys., Vol. 42, pp. 1785-1790.

Muntz, E. P., 1962, "Static Temperature Measurements in a Flowing Gas", Phys. Fluids, Vol. 5, pp. 80-90.

Myerson, A. L., and Watt, W. S., 1968, "Atom Formation Rates behind Shock Waves in Hydrogen and the Effect of Added Oxygen", J. Chem. Phys., Vol. 49, pp. 425-433.

Ocheltree, S. L., and Storey, R. W., 1973, "Apparatus and Techniques for Electron Beam Fluorescence Measurements", Review Sci. Inst., Vol. 44, p. 367.

Peeters, J., and Mahnen, G., 1973, "Reaction Mechanisms and Rate Constants of Elementary Steps in Methane-Oxygen Flames", Symp. (Int.) Combust, 14th, pp. 133-141.

Peterson, R. B., 1988, "Improved Direct Sampling Electron Impact Fluorimetry Apparatus for Combustion Systems", Rev. Sci. Inst., Vol. 59, p. 815.

Peterson, R. B., Lucas, D., Hurlbut, F. C., and Oppenheim, A. K., 1984, "Molecular Beam Overrun in Sampling Transient Combustion Processes", J. Phys. Chem., Vol. 88, pp. 4746-4749.

Robben, F. and Talbot, L., 1966, "Measurement of Shock Wave Thickness by the Electron Beam Fluorescence Method", Phys. Fluids, Vol. 9, pp. 633-643.

Scott, J. E., and Drewry, J. E., Characteristics of Aerodynamic Molecular Beams", Rarefied Gas Dynamics (J. Laurmann, Ed.), 1963, Vol. 1, p. 516.

Shadday, M. A., Kauzlarich, J. J., and Lowry, R. A., 1978, "Total Temperature Probe Calibration in Supersonic Rarified Flows", ASME publication 78-WA/HT-1.

Shumacher, B. W. and Gadamer, E. O., 1959, "Electron Beam Fluorescence Probe for Measuring the Local Density in a Wide Field of Observation", Can. J. Phys., Vol. 36, pp. 659-671.

Smith, O. I., 1982, "Molecular Beam Sampling from Combustion Systems", Paper 82-49, Western States Section of the Combustion Institute, 1982.

Thielen, K., and Roth, P., 1987, "Resonance Absorption Measurements of N, O, and H Atoms in Shock Heated HCN/O_2/Ar Mixtures", Combust. Flame, Vol. 69, pp. 141-154.

Wiese, W. L., Smith, M. W., and Glennon, B. M., 1966, Atomic Transition Probabilities, National Standard Reference Data Series - National Bureau of Standards.

Winkler, E. V., 1954, "Design and Calibration of Stagnation Temperature Probes for use at High Supersonic Speeds and Elevated Temperatures", J. Appl. Phys., Vol. 25 (2), pp. 231-232.

Zaidel, A. N., 1970, Vacuum Ultraviolet Spectroscopy, Ann Arbor-Humphrey Scientific Publishing, pp. 312.

APPENDIX

Appendix A

Program for Calculating Absorption Fractions

This appendix presents a copy of the program ABSORB.FOR. This program was used to calculate the absorption fraction of resonant radiation by either Kr or H atoms in a sample.

```
      PROGRAM ABSORB
      DIMENSION VIE(200) , VIA(200), VINEW(200) , VTEMP(200)
      CHARACTER*6  , FNAME
      CHARACTER*8  , FNAMEX
      CHARACTER*2  , EXT1,EXT2,EXT3,EXT4,EXT5,EXT6,EXT7,EXT8,PRE
      CHARACTER*10 , FNAMEL,FNAMEH,FNAMEV,FNAMEC,FNAMEI
      CHARACTER*10 , FNAME0,FNAME1,FNAME2
      DOUBLE PRECISION ABSCENJ, ACJOLO, ABSCENL
      PRINT*, ' THIS PROGRAM CALCULATES THE DEGREE OF ABSORPTION '
      PRINT*, ' BY GASES IN THE FLOW TUBE FOR SPECIFIED LEVELS OF '
      PRINT*, ' CENTERLINE SELF ABSORPTION IN THE LAMP AND CENTERLINE'
      PRINT*, ' ABSORPTION IN THE FREE JET '
c
C     input variables from the keyboard
c
      PRINT*, '  '
      PRINT*, ' INPUT THE ASSUMED TEMPERATURE OF THE EMITTER '
      READ*, TE
      PRINT*,TE
      PRINT*, ' INPUT THE ASSUMED TEMP OF THE SELF-ABSORPTION '
      READ*, TA
      PRINT*,TA
      PRINT*, ' INPUT THE CENTERLINE SELF-ABSORPTION FRACTION '
      READ*, ABSCENL
      PRINT*,ABSCENL
      PRINT*, ' INPUT THE CENTERLINE JET ABSORPTION FRACTION '
      READ*, ABSCENJ
      PRINT*,ABSCENJ
      ACJOLO=ABSCENJ
c
c
C HYDROGEN AND KRYPTON SELECTION
C
      PRINT*,' INPUT 1 FOR HYDROGEN AND 2 FOR KRYPTON ABSORPTION '
      READ*, GAS
      IF (GAS.EQ.2)THEN
      V0=80972.0
      XM=83.8
   40 FORMAT(' KRYPTON ')
      PRINT*,' KRYPTON'
      ELSE
      V0=100000000/1215
      XM=1
      PRINT*,' HYDROGEN'
      ENDIF
C
C
C CALCULATION OF LAMP PROFILE
C
      CALL SUBSTEP(TE,V0,XM,STEP)
      CALL DOPPLER (TE,V0,XM,VIE,VD1,STEP)
      CALL DOPPLER (TA,V0,XM,VIA,VD2,STEP)
      CALL ABSORP (VIE,VIA,VINEW,ABSCENL,STEP)
      VEZERO=VINEW(1)
      DO 100 I=1,200
```

```
      VIE(I)=VINEW(I)/VEZERO
  100 CONTINUE
      DO 101 I=1,100
      IP=99 + I
      IM=101-I
      VTEMP(IP)=VIE(I)
      VTEMP(IM)=VIE(I)
  101 CONTINUE
      CALL INTEG(VIE,EAREA,STEP)
C
C
C  THIS SECTION PROVIDES FOR THE SELECTION OF A LOW
C  TEMPERATURE AND PRESSURE (INITIAL CONDITIONS)
C  THEN ALLOWS CONDITIONS AT A LATER TIME TO BE INPUT.
C  THIS IS DONE SO THE USER DOES NOT NEED TO CALCULATE
C  SAMPLE ABSORPTION VALUES THROUGH OUT THE EVENT.
C
      PRINT*,' INPUT LOW TEMPERATURE FOR JET '
      READ*,LOWT
      TC=LOWT
      PRINT*,' INPUT HIGH TEMPERATURE FOR JET '
      READ*, HIGHT
      PRINT*, ' INPUT INITIAL PRESSURE '
      READ*,LOWP
      PRINT*, ' INPUT SECOND PRESSURE '
      READ*,HIGHP
C
C
C  THE SAMPLE ABSORPTION AT THE INITIAL CONDITIONS IS FOUND
      j=0
  190 CALL DOPPLER(TC,V0,XM,VIA,VD3,STEP)
      CALL ABSORP(VIE,VIA,VINEW,ABSCENJ,STEP)
      CALL INTEG(VINEW,AAREA,STEP)
      ABSTOT=(EAREA-AAREA)/EAREA
      TJ=J*.1
      PRINT*, 'LOWP= ',LOWP,' T= ',TC,' ABSORPTION= ',ABSTOT
      IF(J.EQ.0)THEN
        DO 265 I=1,100
        IM=101-I
        IP=99+I
        VTEMP(IP)=VINEW(I)
  265   VTEMP(IM)=VINEW(I)
      ENDIF
C
C
C  THE SAMPLE ABSORPTION AT THE SECOND TIME IS FOUND
      J=J+1
      IF(J.EQ.1)ACJOLD=ABSCENJ
      IF(J.EQ.1)TC=HIGHT
      IF(J.EQ.1)TTT=HIGHP/LOWP*(LOWT/HIGHT)**1.5
      IF(J.EQ.1)ABSCENJ=1-(1/(EXP(TTT*LOG(1/(1-ACJOLD)))))
      print*,' abscenj= ',ABSCENJ
      IF(J.GE.2)GO TO 290
      GO TO 190
  290 CONTINUE
```

```
      DO 220 I=1,200
      XI=(I-1)*STEP
      X2I=100000000/(V0-XI)-(100000000/V0)
  220 CONTINUE
      END
C
C
C  THIS ROUTINE CALCULATES THE STEP SIZE FOR NUMERICAL INTEGRATIONS
C
      SUBROUTINE SUBSTEP(T,V0,XM,STEP)
      STEP=(7.162*V0*SQRT(T/XM)/10**7)/50
      RETURN
      END
C
C
C  THIS ROUTINE CALCULATES THE DOPPLER PROFILE FOR THE INPUT
C  TEMPERATURE
C
      SUBROUTINE DOPPLER(T,V0,XM,VI,VD,STEP)
      DIMENSION VI(200)
      VD=7.162*V0*SQRT(T/XM)/10**7
      PRINT*,' VDLAMP= ',VD,' V0= ',V0
      DO 10 I=1,200
   10 VI(I)=0
      I=0
   20 I=I+1
      VI(I)=EXP(-2.773*(((I-1)*STEP)/VD)**2)
      IF(VI(I).GT..00001)GO TO 20
      RETURN
      END
C
C
C  THIS ROUTINE CALCULATES THE PROFILES AFTER ABSORPTION
C
      SUBROUTINE ABSORP(VIE,VIA,VINEW,ABSCEN)
      DIMENSION VIE(200),VIA(200),VINEW(200)
      DOUBLE PRECISION ABSCEN
      VAZERO=VIA(1)
      XX=LOG(1-ABSCEN)/VAZERO
      DO 10 I=1,200
   10 VINEW(I)=VIE(I)*EXP(VIA(I)*XX)
      RETURN
      END
C
C
C  THIS ROUTINE INTEGRATES INTENSITIES
C
      SUBROUTINE INTEG(VI,AREA,STEP)
      DIMENSION VI(200)
      AREA=0
      DO 10 I=1,199
      IP=I+1
   10 AREA=((VI(I)+VI(IP))/2)*STEP+AREA
      RETURN
      END
```